# Observations of the initiation and evolution of the 2001 Mars global dust storm

Melissa J. Strausberg

Department of Atmospheric and Oceanic Sciences, University of California, Los Angeles, Los Angeles, California, USA

Division of Geological and Planetary Sciences, California Institute of Technology, Pasadena, California, USA

Huiqun Wang, Mark I. Richardson, and Shawn P. Ewald

Division of Geological and Planetary Sciences, California Institute of Technology, Pasadena, California, USA

Anthony D. Toigo

Graduate School of Science and Technology, Kobe University, Kobe, Japan

Center for Radiophysics and Space Research, Cornell University, Ithaca, New York, USA

[1]   A global dust storm occurred on Mars between June and October 2001. The storm began near Hellas just before southern spring equinox ($\sim L_s = 177°$). Local storms, likely forced by a combination of slope-flow and ice cap thermal contrasts, were observed to propagate along the northwestern rim of Hellas, apparently triggering the global storm. Cap-edge storm activity for much of late southern winter was similar in 2001 to one Mars year earlier; however, a very large storm propagated into the basin just after $L_s = 177°$. Subsequently, the total area of storm activity in 2001 was roughly double that of the previous year. For about 10 days, dust lifting was limited to the Hellas region. As additional storms propagated into Hellas, activity built and extended northward into Syrtis and eastward into Hesperia. It is not clear whether transport or spreading of lifting were of greatest importance for expansion. At $L_s = 185°$ the storm began to spread rapidly to the east, along a line from the southern pole to the northern tropics. Essentially no storm propagation to the west occurred, yielding strong zonal asymmetry of expansion. As the dust storm reached the western edge of Tharsis, secondary dust lifting centers developed in Daedalia and Solis (southeastern Tharsis). Subsequently, the storm rapidly encompassed the planet (by $L_s = 193°$). Once fully global, the Syria/Solis/Daedalia lifting center appeared to dominate (on the basis of cloud top morphology), with Hellas quiescent. By $L_s = 212°$, lifting could no longer be discerned. Thereafter, dust haze appeared uniform and diffuse, and decay appeared to have set in.

**Citation:**   Strausberg, M. J., H. Wang, M. I. Richardson, S. P. Ewald, and A. D. Toigo (2005), Observations of the initiation and evolution of the 2001 Mars global dust storm, *J. Geophys. Res.*, *110*, E02006, doi:10.1029/2004JE002361.

## 1.   Introduction

[2]   A Martian global dust storm is one of the most dramatic, dynamical phenomena in the solar system. Over the course of a few weeks, dust is swept into the atmosphere to form a veil that almost completely enshrouds the planet [*Fernandez*, 1997; *Kahn et al.*, 1992; *Martin*, 1973; *Thorpe*, 1979; *Wang and Ingersoll*, 2003]. Lifting of dust in these storms is likely not globally uniform, and thus the term "planet-encircling" has been coined [*Martin and Zurek*, 1993] (we chose to use the term "global" since the dust encompasses most or all of the planet, distinguishing these storms from regional or local events). Global storms are variable phenomena.

Through telescopes and from orbiting spacecraft, it has been possible to note their occurrence in some Martian years, but not others, while the specific seasonal date of occurrence varies for the years in which they do occur [*Martin and Zurek*, 1993]. Some consistency in global dust storm development exists: such storms have only been observed to occur during southern spring and summer, when Mars is nearer to perihelion.

[3]   Dust storms are of great importance for the Martian climate. The dust is a mineral aerosol that absorbs and scatters both solar visible and planetary infrared radiation, modifying the radiative heating of the atmosphere and surface. The dust, which is thermally coupled with the atmosphere, is also an emitter of infrared radiation, increasing the effective emissivity of the atmosphere. During global dust storms, the air temperatures can increase at mid-levels ($\sim 25$ km) by many tens of degrees [*Conrath*,

1975; *Leovy*, 1985; *Smith et al.*, 2002], while the shading of the surface due to the largest global dust storm of 1977 caused a roughly 10 K decrease in daytime near-surface temperatures [*Ryan and Henry*, 1979].

[4] The origin of global dust storms is poorly understood. Inspection of images strongly suggests that near-surface winds causes lofting of dust. These initial strong winds may be generated by thermal contrasts near the cap edge [*Burk*, 1976; *Haberle et al.*, 1979; *Leovy et al.*, 1973; *Siili et al.*, 1997; *Toigo et al.*, 2002], large slopes [*Magalhaes and Young*, 1995; *Siili et al.*, 1997], fronts associated with low pressure storms [*Leovy*, 1972; *Wang et al.*, 2003], or by variations in other atmospheric waves or circulation systems. In some circumstances, the small dust storms resulting from strong winds, which develop relatively frequently on Mars in years with and without global dust storms [*Cantor et al.*, 2001; *Peterfreund and Kieffer*, 1979], blow up into larger storms, with some developing into full global storms. It is suspected that a feedback develops wherein increased atmospheric heating results in stronger circulation and hence increased dust lifting. Numerical models indeed show that such feedback on the general circulation is likely [*Haberle et al.*, 1982]. The specific dynamical mechanisms of feedback are not understood. It has been suggested that these take the form of "dusty" equivalents of hurricanes [*Gierasch and Goody*, 1973]; that the increased dust modifies the propagation and amplitude of atmospheric waves such that winds are increased [*Leovy et al.*, 1973; *Tillman*, 1988; *Zurek and Leovy*, 1981]; or, that the increased dust loading causes dramatic transitions in the extent of meridional circulation cells [*Schneider*, 1983].

[5] Prior to the Mariner 9 mission in 1971, global dust storms had been observed as periods of obscuration in telescopic images [*Briggs et al.*, 1979; *Martin and Zurek*, 1993]. Some idea of initiation sites could be obtained from these images, as well as the relative size of events in different years. Spacecraft observations have dramatically increased both the quality and resolution of dust storm observations. Mariner 9 arrived at Mars during a very large event, and was not able to obtain clear pictures of the surface for many weeks. The Mariner 9 camera observations of the limb provided observations of how deeply dust was spread in the vertical (up to 70 km [*Anderson and Leovy*, 1978]), while thermal observations allowed the impact of the storm on atmospheric temperatures to be assessed [*Conrath*, 1975; *Hanel et al.*, 1972; *Leovy*, 1972; *Wilson and Richardson*, 2000]. The Mariner 9 thermal infrared observations have subsequently been used to retrieve the evolving pattern of dust optical depth during the decay phase of this storm [*Fenton et al.*, 1997; *Liu et al.*, 2003]. The Viking mission from 1976–1980 observed two global dust storms in 1977 from twin orbiter and twin landers. The lander data yielded insight into the atmospheric response to the dust storm [*Zurek and Leovy*, 1981], the impact on near surface air temperatures [*Ryan and Henry*, 1979], and on the pattern of surface winds [*Haberle et al.*, 1982]. The orbiters obtained information on the global air temperature changes, including the development of a substantial warming of the winter polar atmosphere at the peak of the storm [*Jakosky and Martin*, 1987; *Martin and Kieffer*, 1979; *Wilson*, 1997; *Wilson and Richardson*, 2000]. The infrared data were also used to retrieve dust opacity distributions [*Liu et al.*, 2003;

*Martin*, 1986; *Martin and Richardson*, 1993]. Unlike the Mariner 9 mission, the Viking observations caught the inception as well as the evolution and decay of two global dust storms during a single year. Imaging of local storms prior to the global events was possible, but due to the limited field-of-view of the camera and downlink constraints, coverage of the storm initiation was far from complete [*Briggs et al.*, 1979].

[6] Mars Global Surveyor (MGS) went into orbit about Mars in late 1997. Unlike Mariner 9 and the Viking Orbiters, MGS is in a nearly circular, sun-synchronous (2 pm−2 am) orbit [*Albee*, 2000]. From this orbit, regular coverage of the planet is possible. MGS carries two instruments of primary interest for this study, the Thermal Emission Spectrometer (TES), which provides nearly continuous measurement of the infrared spectrum between 7 and 50 $\mu$m with a spectral resolution of about 10 cm$^{-1}$, a spatial resolution of about 6km, and an across-track coverage of $\sim$20 km [*Christensen et al.*, 1992, 2001], and the Mars Orbiter Camera (MOC), which obtains continuous, two color images with a resolution of about 7.5 km and nearly limb-to-limb across-track coverage [*Malin*, 1992; *Malin and Edgett*, 2001].

[7] In the almost three Mars years since insertion into Martian orbit [1997], MGS has observed one global dust storm. This storm began in late June, 2001. The consistency, quality, and volume of coverage of the 2001 event make it the most well documented Martian global dust storm. The TES observations have been described by *Smith et al.* [2002], while the MOC data have not been described in the literature (though they were briefly discussed in several conference abstracts [*Cantor and Malin*, 2003; *Malin and Cantor*, 2003]). In this paper, we examine both the MOC data and aspects of the TES data not described by *Smith et al.* [2002]. The goal is to develop a description of the storm that may be used to constrain model and theory of storm development. To better understand the initiation of the dust storm and the inter-annual variability of the Martian dust cycle, we examine spring south polar cap edge storms in both 1999 and 2001 and the increase in dust lifting activity in the Hellas basin. To understand the transition between local or regional and global dust storms, we consider dust transport from Hellas, the development of secondary dust lifting centers in other regions of the planet and how changes in the general circulation of the atmosphere relate to these events.

[8] In the next section, we more completely describe the MGS instrument data sets used in this study, and the processing of these data. We then proceed to provide an overview of the 2001 storm as context for the remaining discussion. In section 4, we review south polar cap edge activity just prior to the 2001 storm, and compare it with activity in the preceding year. In section 5, the evolution of the storm is examined. We conclude with a summary.

## 2. Types of Observations

### 2.1. Mars Orbiter Camera

[9] The majority of the data used in this study is derived from the twin Mars Orbiter Camera (MOC) Wide-Angle (WA) cameras. The two WA cameras, one each to provide

red and blue images, along with the MOC Narrow-Angle camera compose the imaging capability of MGS [*Malin*, 1992]. The WA cameras are push-broom systems with an across-track field of view that is effectively limb-to-limb. The peak spatial resolution at the subspacecraft point is ~250 m, although the cameras can be read-out at decreased resolution to reduce down-link volume. Atmospheric observations from the MOC WA cameras has been described by *Cantor et al.* [2001, 2002] and *Wang and Ingersoll* [2002, 2003]. The processing necessary to use the WA daily global images in color is described by *Wang and Ingersoll* [2002], and the same procedure is used in this study. The MOC data used in this study were taken from the Planetary Data System (PDS).

### 2.1.1. Daily Global Images

[10] Daily Global Map (DGM) images are obtained by both WA cameras as continuous strips on the day-side portion of each orbit [*Wang and Ingersoll*, 2002]. The variation in across-track resolution is eliminated by differential summing across the detector such that roughly 7.5 km pixels are obtained (during the dust storm, most images were acquired at 3.75 km/pixel). The DGM WA images were separately processed, including radiometric and photometric correction, as well as map projected using custom routines. Simple cylindrical projection was chosen for these images because of their vast latitudinal extent. The color channels were combined and the images mosaicked to produce regional and global maps. "Seams" in the DGM images (Figure 1) result not from variations in resolution, but from the increased blurring due to increased atmospheric opacity at high viewing angles (on the planetary limb). In some cases, the images were manipulated, in terms of colors, brightness, and contrast, using desktop image manipulation software (GIMP and Photoshop) for clarity.

### 2.1.2. Regional Wide-Angle Images

[11] The MOC WA cameras can be read-out with pixel sizes as small as ~250 m. Such images were acquired for nearly the entire planet at the beginning of the MGS mapping mission in what was called the "geodesy" campaign [*Caplinger and Malin*, 2001]. WA context images are taken in conjunction with many of the MOC NA angle images, while other non-DGM WA images are acquired for other reasons, including a large number for the purpose of studying the atmosphere.

[12] The regional WA images included in this study were collected only with the red WA camera. They typically were collected with ~930 m per pixel and a "footprint" of approximately 1700 km by 1900 km. These images clearly show the detailed structures of dust storms and clouds. For this study, the regional wide-angle images were used to examine polar cap edge storm activity, primarily in the Hellas region, to track the origin of the 2001 global dust event. No regional wide-angle images are available for the latter part of the 2001 global dust event (after $L_s = 188$). Regional wide-angle coverage of Hellas was sparse for southern spring in 1999, making year-to-year comparison within this data set difficult.

[13] As with the daily global images, processing was accomplished using the ISIS suite. These images were examined in polar projection, which is most appropriate for images so close to the pole. Cropping and adjustment of brightness and contrast in the final images were performed using a desktop image manipulation program.

### 2.2. Thermal Emission Spectrometer Observations

[14] TES provides infrared data simultaneous with the subspacecraft portions of the MOC WA images (1–2 pixels wide for the DGM WA images and ~8 pixels wide for the regional WA images). The instrument provides spectral information across the thermal infrared spectrum ($\sim$7–50 $\mu$m) at moderate spectral (10 cm$^{-1}$) and spatial ($\sim$6 km) resolution [*Christensen et al.*, 1992, 2001]. The data have been used to derive profiles of atmospheric temperature [*Conrath et al.*, 2000] and aerosol opacities [*Smith et al.*, 2000]. The evolution of the 2001 dust storm has been described using this data by *Smith et al.* [2002]. As such, our inclusion of TES data in this study is limited.

[15] For this study, we make use of the temperature and opacity results derived by *Conrath et al.* [2000] and *Smith et al.* [2000] and included on the TES PDS archive. In addition, we use TES spectra which have been convolved with the Viking Infrared Thermal Mapper 15-$\mu$m channel spectral response function [*Liu et al.*, 2003; *Martin and Kieffer*, 1979; *Wilson and Richardson*, 2000]. In this form, the data provides a gauge of bulk atmospheric temperatures between ~10 and 40 km, centered at 25 km [see *Wilson and Richardson*, 2000, Figure 1].

## 3. Overview: 2001 Global Dust Storm Evolution

[16] Imaging and thermal data illustrating the evolution of the 2001 global dust storm are shown in Figures 1 and 2. In late northern autumn (prior to $L_s \approx 170°$, where $L_s$ is the seasonal indicator, measured in degrees from $L_s = 0°$ at northern spring equinox), atmospheric behavior in 2001 was very similar to that in the previous Martian year. Water ice clouds were visible, associated with the Tharsis volcanoes, but the atmosphere was otherwise quite clear. During this period, local dust storms with lifetimes of hours to days occurred at various longitudes in the southern hemisphere in the vicinity of the southern seasonal polar cap edge. An example of such a storm can be seen in the region of Hellas in Figure 1b. These storms were predominantly stationary during their lives and rarely, if ever, grew beyond their immediate area of origin. Their occurrence in the previous year (the first MGS mapping year) has been extensively documented by *Cantor et al.* [2001]. Dust lifting in these storms likely was initiated by strong winds driven by the strong thermal contrast (tens-of-degrees Kelvin) between the seasonal $CO_2$ cap and the adjacent ice-free ground (section 4.1.1). The degree of similarity in these "cap-edge" storms between the first and second MGS mapping year is examined in detail in section 4.1.

[17] After $L_s = 170°$, a seasonal cap edge storm, initially to the southwest of the Hellas basin, traveled north and eastward along the western rim of the basin. Additional lifting subsequently developed in and then around Hellas, as is apparent in both the visible (Figure 1c) and thermal (Figures 2e–2h) data. Pronounced dust lifting became common after $L_s \sim 182°$. The tops of these dust clouds resemble convective clouds in the Earth's atmosphere, and suggest active mixing and lifting (see discussion in section 4.1). At this time, both dust opacity and mid-level
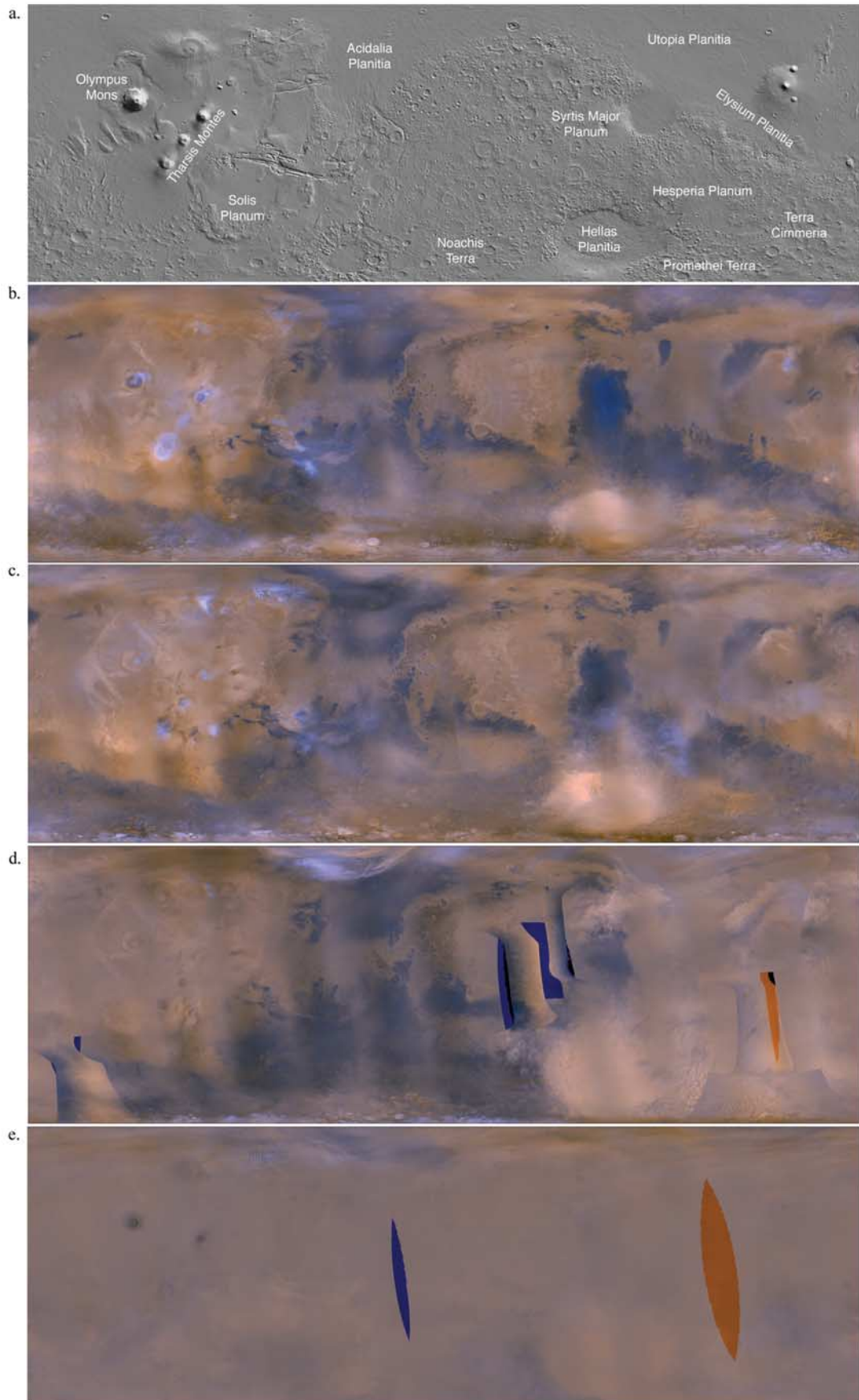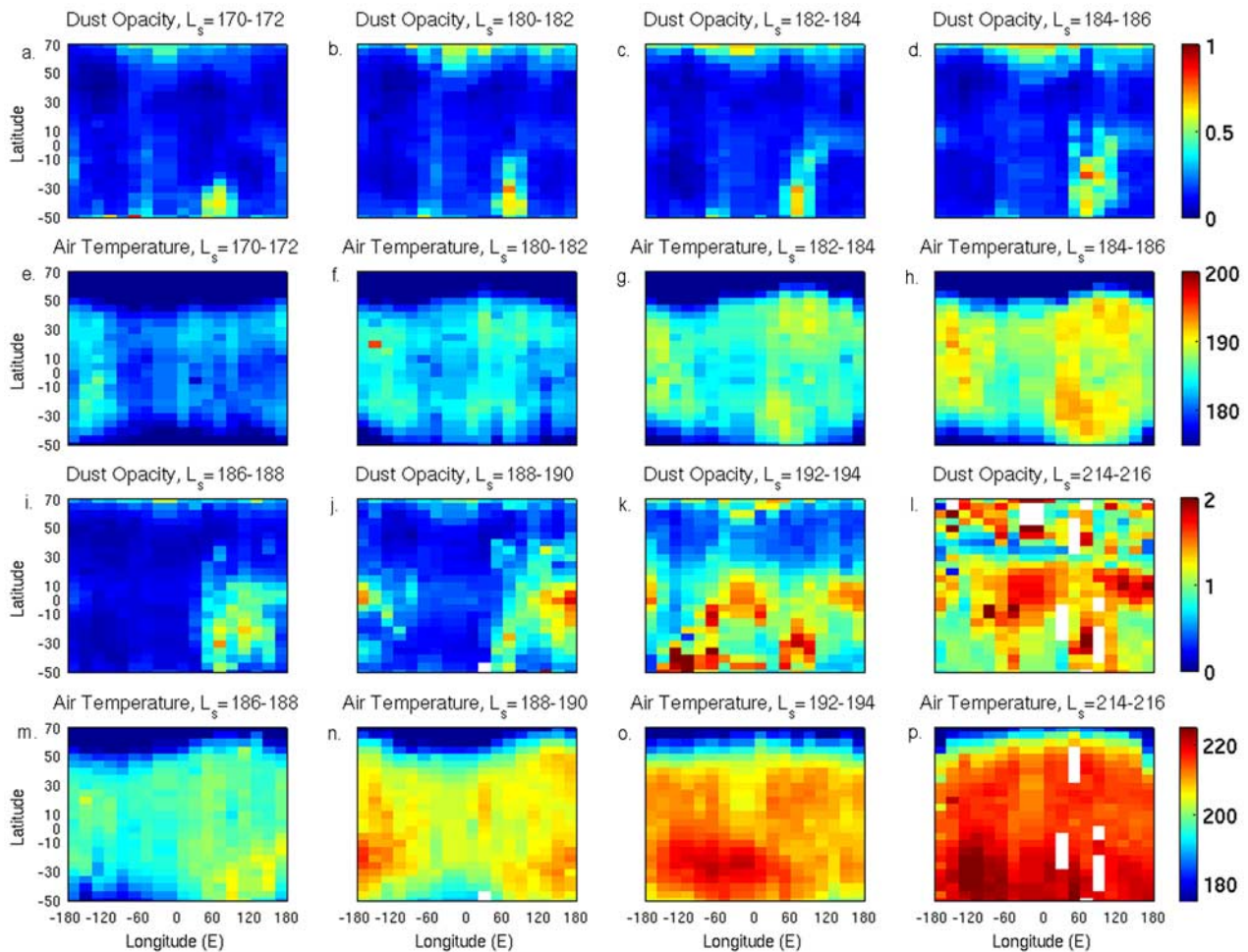
**Figure 1**

**Figure 2.** MGS TES data showing local changes in opacity and 15 μm absorption before, during, and after the 2001 global dust storm. Data were placed in longitude bins of 20° and latitude bins of 5°. Each frame represents 5° of $L_s$. Data that were flagged by the TES team as being of low quality were excluded, as were temperatures and opacities outside of the physically reasonable values; acceptable temperatures were from 100 K to 300 K, and acceptable opacities were from 0 to 20.

(0.5 mbar) air temperature in the region of Hellas increased noticeably relative to the surrounding areas.

[18] Between $L_s = 182°$ and $L_s = 185°$, the storm began to expand out of Hellas. It initially expanded northward in pulses (expansions of the dust cloud edge northward over a day or so), which were subsequently entrained in an eastward flow. After $L_s = 185°$, there were two distinct spurs of dust transport: across the equator into Syrtis, and northeastward into Hesperia. The evolution of optical depth to the northeast of Hellas during this period has already been described by *Smith et al.* [2002] and *Liu et al.* [2003]. During this period, the air temperatures became more zonally uniform (the elevated temperatures were no longer tightly constrained to the Hellas basin longitudinal sector).

[19] Between $L_s = 185°$ and $L_s = 188°$ dust spread rapidly eastward across Hesperia and northern Cimmeria. One major pulse of dust moved north of Syrtis during this period, appearing as a secondary storm in the TES observations [*Smith et al.*, 2002], before moving to the east and dissipating. Although several significant pulses of dust were observed to develop on the on the highlands to the west of Hellas, no significant sustained expansion of the storm occurred in that direction. This lack of westward progress is also obvious in the TES optical depth data [*Smith et al.*, 2002]. The asymmetric expansion of the storm is a major characteristic of this planet-encircling storm that is in need of explanation. During this same period, a major dust cloud was observed to

**Figure 1.** Evolution of the 2001 global dust storm as shown in MGS MOC daily global weather maps, mosaicked from 12 image swaths taken across the planet at 2 pm local time each day. The images shown extend from 60°S to 60°N latitude and from −180° to 180°E longitude. (a) MOLA topography for reference; (b) early polar cap edge storms near Hellas basin ($L_s = 170°$); (c) convective-type dust lifting in Hellas basin ($L_s = 183°$); (d) the start of a secondary dust lifting center near Tharsis Montes ($L_s = 188°$); (e) the entire planet encircled by a thick layer of atmospheric dust ($L_s = 212°$).

travel south from the Hellas basin, over the seasonal cap, and by $L_s = 190°$, the residual cap (Figure 3). The initial southward "break out" of this dust from Hellas began at about $L_s = 186°$, about a day or so after the beginning of the major dust advance across Hesperia. This southern polar dust traveled fully across the cap by $L_s = 193°$, and was no longer distinguishable from the much elevated background dust opacities by $L_s = 198°$.

[20] Although dust was being transported across Hesperia to the east and had reached the western edge of the Tharsis plateau by $L_s = 188°$, both the imaging and the TES optical depth data [*Liu et al.*, 2003] indicate the activation of a secondary dust lifting center in Daedalia Planum, just south and east of the Tharsis ridge shield volcanoes Pavonis and Arsia Mons. This secondary center became active before the dust opacity on the eastern side of Tharsis rose rapidly. It appears clearly as a detached opacity maximum in the TES data (Figures 2j and 2k) and immediately preceded the rapid storm growth to global encircling scale (by $\sim L_s = 190°$). Following $L_s = 190°$, the global optical depth increased to a storm peak sometime around $L_s = 205°$ [*Smith et al.*, 2002]. The Syria/Solis/Daedalia lifting center remained active after other centers had apparently switched off (on the basis of dust cloud top morphology), out to about $L_s = 220°$. Storm decay set in at different times at different latitudes, before $L_s = 200°$ in the southern lower midlatitudes [*Smith et al.*, 2002].

[21] The overview of the 2001 dust storm provided by the MOC DGM images (this study) and the TES dust optical depths [*Liu et al.*, 2003; *Smith et al.*, 2002] suggests some interesting issues for more detailed examination: (1) the relationship between cap edge dust storms and the initiation of the 2001 storm, (2) growth of the dust storm in Hellas, (3) transport of dust across Hesperia to the east of Hellas, but not across Noachis to the west, (4) the activation of the major secondary dust lifting center in Daedalia, and (5) the evolution of dust lifting centers after global expansion of the storm.

## 4. Seasonal Cap Edge Storms and Global Storm Initiation

### 4.1. Initiation of the 2001 Global Dust Storm

[22] Inspection of the DGM MOC WA images (Figure 1) and the mapped TES dust optical depth data (Figure 2) demonstrate that the 2001 global dust storm began in the region containing the Hellas basin [*Liu et al.*, 2003; *Smith et al.*, 2002]. This region has historically been associated with the initiation of large dust storms [*Briggs et al.*, 1979]. The rim of Hellas provides significant relief to drive slope winds [*Magalhaes and Young*, 1995; *Siili et al.*, 1997], the surface pressure is high promoting dust suspension [*Greeley*, 1992], and at the equinoctial season of the 2001 dust storm the presence of the seasonal cap edge in the proximity of Hellas provided a strong thermal drive for "sea-breeze"-like circulations [*Burk*, 1976; *Siili et al.*, 1997; *Toigo et al.*, 2002]. The 2001 observations are by far the best documentation of the initiation of a global dust storm on Mars. The combination of excellent coverage and relatively high resolution make the MOC DGM images the best means of documenting this initiation and testing the initiation mechanism hypotheses.

[23] The day-to-day variation of dust activity in the Hellas basin region from $L_s = 177°$ to $L_s = 185°$ is shown in Figures 4a–4m. At the beginning of this sequence, a large local storm could be seen to the west of Hellas and just north of the seasonal cap edge (Figure 4a). By the next day, the dust storm was located on the western rim of Hellas (Figure 4b; also in this frame a separate local storm on the eastern rim of Hellas is suggested). While it is not possible to determine for certain whether lifting was ongoing within the storm, two lines of evidence suggest that it was. First, examination of DGM images suggests that such dust clouds can decay to a state where they are hard to distinguish from the surface on time-scales of a day. Lifting within the cloud may be required for the cloud to be seen from day-to-day. Second, the dust cloud in the second frame exhibited crisp edges and sharp cloud top structure reminiscent of terrestrial convective storms. As seen with the global storm (and in other cases), during decay (when lifting has presumably ceased), dust clouds lose this sharp structure and become diffuse. Throughout this paper, we use the observation of such crisp or sharp cloud top structure as evidence of local lifting, but this need not be the case, and is an assumption. These features do suggest higher concentration of dust and vigorous mixing. While this may be analogous to terrestrial rain cloud systems, where the systems are indicative of dynamical processes but necessarily of local (in this case water) sources, the correlation of the regions exhibiting such structure with the regions of highest TES opacities, and the fact that the global storm begins to decay following the termination of such crisp or sharp cloud structure (section 5.3), encourages our interpretation.

[24] A day later, the dust cloud had moved little and appeared somewhat more diffuse. The most sharply defined edge of the storm was now located on the northern rim of the basin. But strongly resurgent activity was indicated the next day, $L_s = 179°$ (Figure 4d). Dust lifting can be seen in this frame along the western rim and extending southwest into southern Noachis and almost to the edge of the seasonal ice cap. In the north, the dust cloud extended out of the basin and northward toward Isidis. A potentially separate and much smaller dust storm could be seen on the southern rim of Hellas and again not far from the seasonal cap edge.

[25] Three days later, at $L_s = 181°$, there was little evidence for active lifting in Hellas except on the northern rim and on the highlands to the north of Hellas. Even here, the clouds showed less sharply defined edges, although the "clumpy" texture of the clouds suggested some convective activity. In the east, dust was being transported eastward (compare Figures 4e and 4a; by $L_s = 181$ the dust completely obscured the terrain to the east of Hellas that had been visible at $L_s = 177°$), but without the significant crisp relief or cloud top structure. By the next day, the eastward transported dust had dissipated somewhat, but in the north activity was elevated (Figure 4f). The northern dust activity continued to build through the rest of the sequence (until $L_s = 185°$, Figure 4l).

[26] Figure 4g shows data from $L_s = 182°$. At this time, another storm was observed to the southwest of Hellas and just north of the seasonal cap. This storm is shown in greater detail in Figure 6b. The propagation of this storm along the western rim of Hellas appears to have caused a flourish of
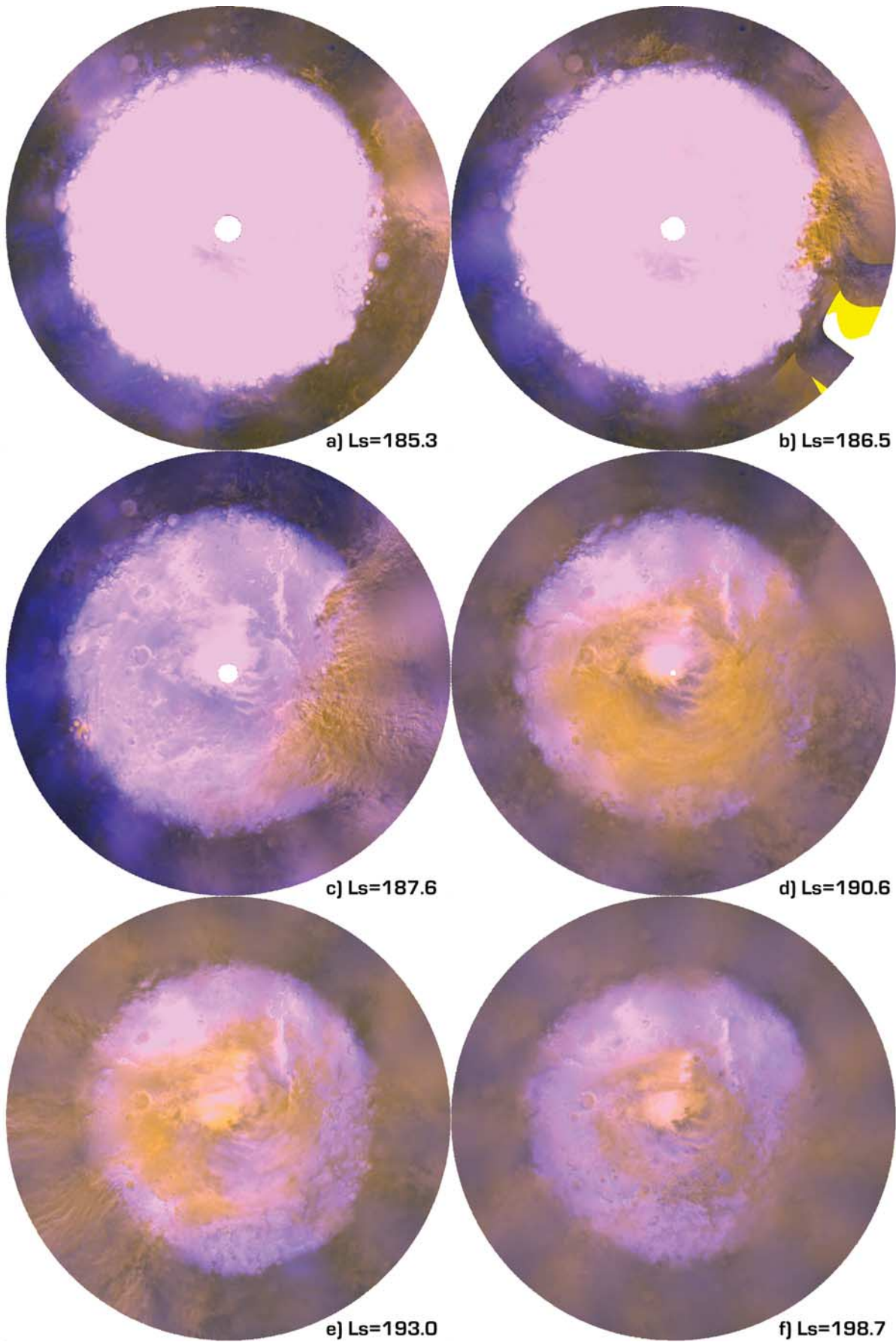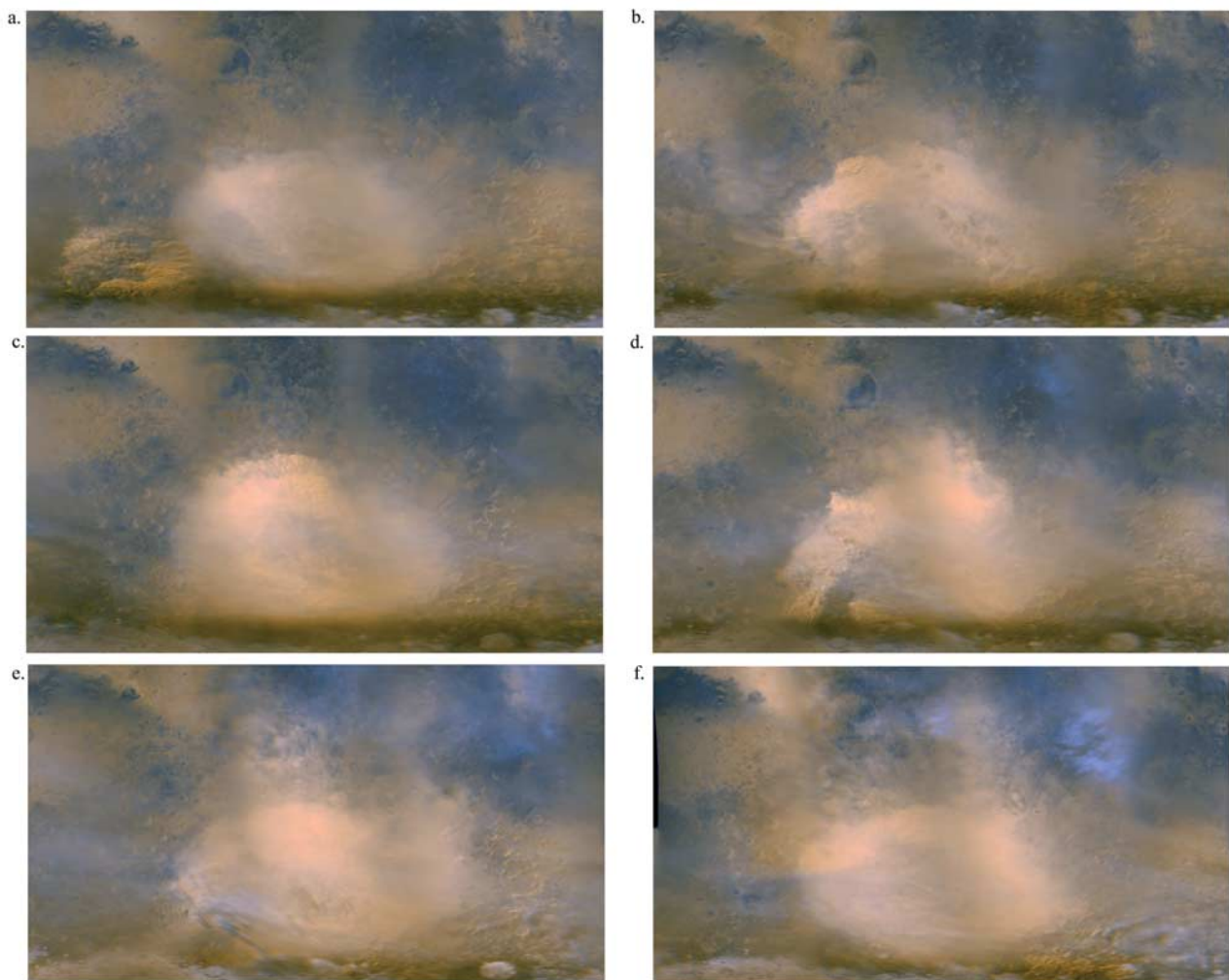
a) Ls=185.3

b) Ls=186.5

c) Ls=187.6

d) Ls=190.6

e) Ls=193.0

f) Ls=198.7

**Figure 3**

**Figure 4.** MOC daily global weather map mosaics of the Hellas region, from $L_s = 178°$ to $L_s = 185°$, showing the progression of dust storm activity in the area from small, isolated storms to large, spreading storms. These images were taken from global maps in simple cylindrical projection. In Figures 4a–4c, individual storms appear short-lived and do not interact appreciably with dust lifting events elsewhere in the region. Beginning in Figure 4d, however, storms appear to circulate around Hellas Basin and grow in the process. The storms continue in this way through Figure 4h. From Figures 4i through 4l these storms grow, and the dust that they have lifted is blown north, out of the Basin. It is this final occurrence that appears to turn a local event into a regional or global one. MOLA topography is provided for reference.

dust lifting in the northwest of the basin the following day. Seasonal cap edge storms were present again three and five days later (Figures 4k and 4l, corresponding to $L_s = 184°$ and $185°$). This dust lifting between Hellas and the seasonal cap edge proceeded for the next few days, and spawned the cloud that was transported across the southern polar cap, as shown in Figure 3.

[27] The dust storm was well on its way to achieving global extent by the time of the final frame of Figures 4a–4m, with extensive clouds of dust extending away from Hellas to the north into Isidis and to the northwest into Hesperia. The image sequence in Figures 4a–4m therefore shows the initiation of the global dust storm as dust was transported out of the Hellas basin.

[28] The image sequence in Figures 4a–4m also shows some evidence of water ice cloud activity at the periphery of the dust storm, as observed for previous storms [*James et al.*, 1994]. To the north and east of Hellas, water ice clouds were indicated by a whitening or bluing of the aerosol clouds in Figures 4d–4k.

[29] A summary of the observations suggests a few key elements for the initiation. First, the propagation of cap edge dust storms from the southwest and along the western edge of Hellas appears to have initiated first lifting of dust in

**Figure 3.** Polar stereographic projections of portions of MOCWA DGM mosaics for seasonal dates indicated on each frame. The sequence shows the propagation of dust over the southern cap during the expansion phase of the 2001 global dust storm.
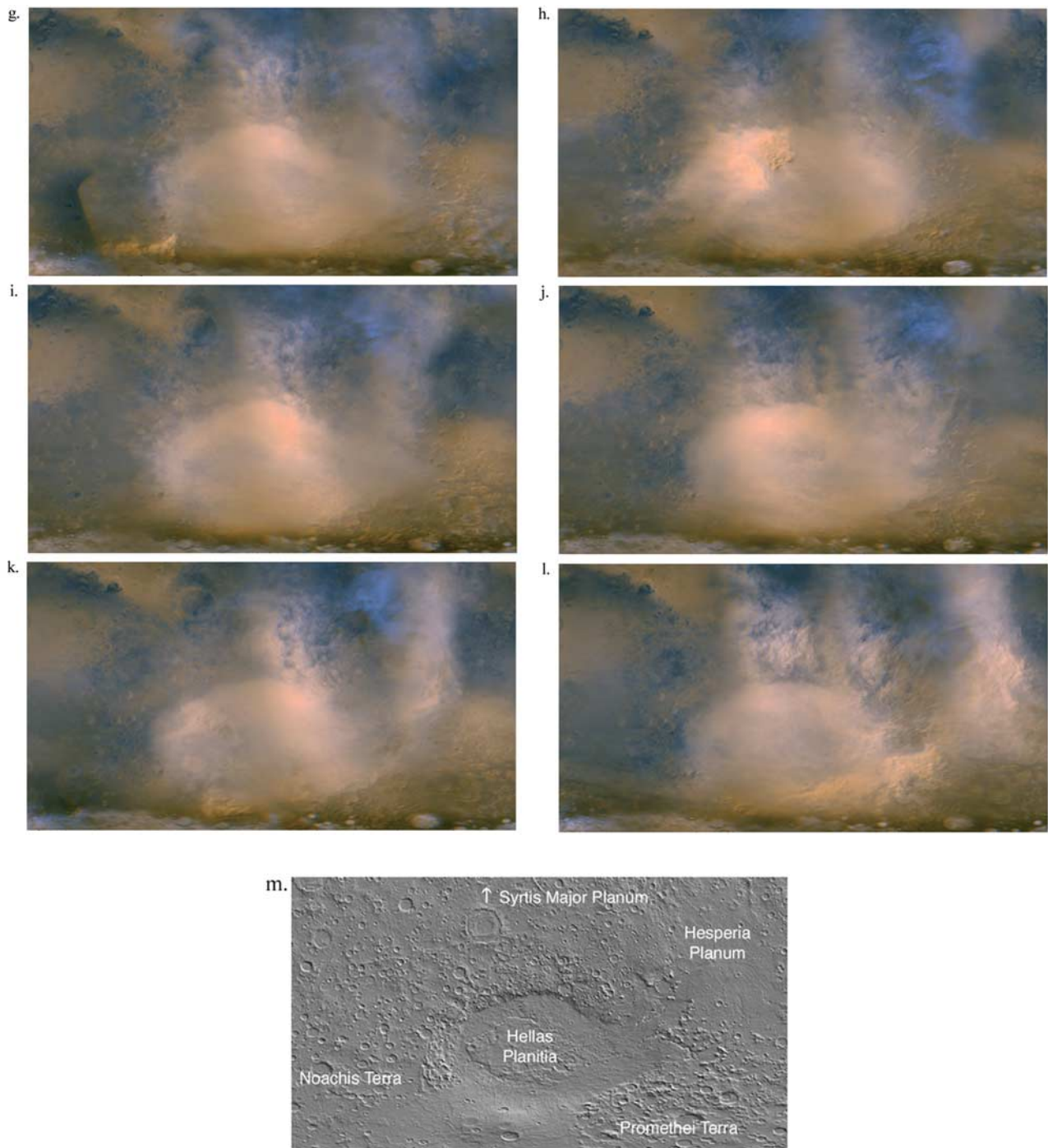
**Figure 4.** (continued)

Hellas at $L_s = 177°$ (this is first date for which behavior is demonstrably different from the year prior), and served to generate secondary sets of lifting events in Hellas on two subsequent occasions. Second, dust lifting on the northern and northwestern edge of Hellas continued throughout the image sequence after initiation at $L_s = 177°$. Sustained lifting on this rim, in conjunction with periodic expansion to the north, may have been critical in providing the sustained increase in dust opacity within Hellas and in "spinning up" the larger scale circulation. Finally, the export of dust out of the basin to the east is seen later in the paper (section 5) to have been critical to the extension of the storm over the southern highland plains of Hesperia, generating the regional-scale phase of the storm. Several sets of diffuse haze were advected to the east before the final vigorous growth after $L_s = 183°$. This vigorous expansion was more crisply defined and may have been associated with the broad eastward advection of dust lifted to the north of Hellas. The cap edge dust storms and dust storms on the western rim of Hellas appear to have been critical factors in the initiation of the 2001 global dust storm.
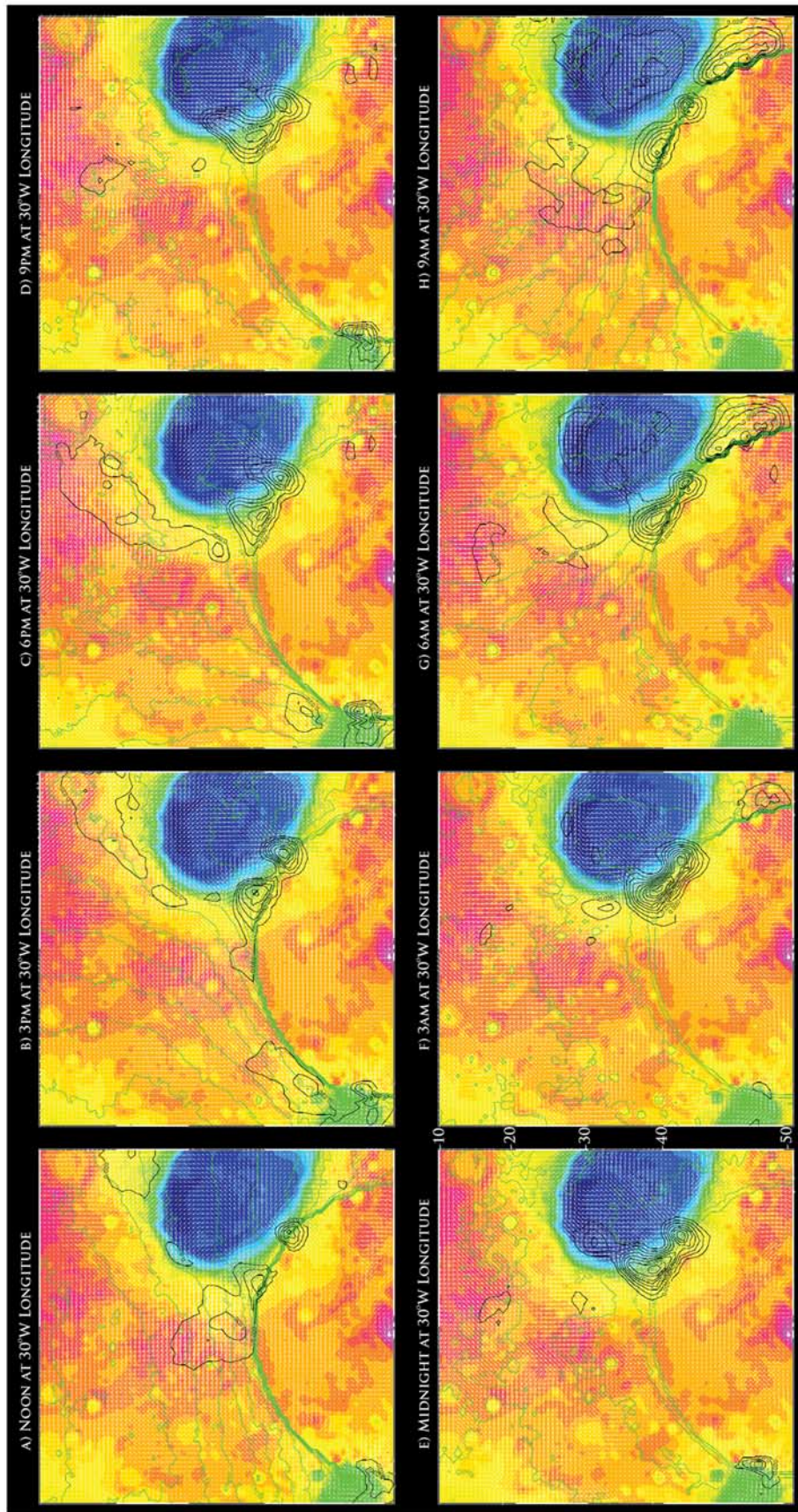
Figure 5

#### 4.1.1. Hellas and Seasonal Cap Edge Wind Stresses at Equinox

[30] Simulations with the Mars MM5 mesoscale model [*Toigo et al.*, 2002] give some indication of why the region to the south and west of Hellas is a favored site for local dust storm activity. Figure 5 shows output at three hour intervals (an hour is here defined as 1/24th of a Martian day) for a single, but representative, day from a simulation run at $L_s = 180°$ with the cap edge location prescribed from observations.

[31] The region to the south of Hellas, and extending further in longitude than the maximum width of the basin, shows persistent elevated wind stresses throughout the diurnal cycle. It is within this region that most of the local storms noted prior to the global storm are observed to have formed. The stresses here are directly related to the thermal contrast across the cap edge and are the result of "sea-breeze" circulations [*Burk*, 1976; *Siili et al.*, 1997; *Toigo et al.*, 2002]. Such cap edge flows occur at all longitudes, but are greatly augmented near Hellas due to the proximity of the sloping southern rim of the basin. Indeed, the model indicates that near-surface winds flowing off the cap are strongly channeled and concentrated as they flow down the slope into the Hellas basin. As the daily cycle progresses, the global tide and differential heating on the slopes of the Hellas basin rim cause the position and strength of the channeled inflow to drift in longitude.

[32] The western rim of the Hellas basin and the highlands just to the west become sites of high wind stress in the afternoon. The winds generating these stresses are themselves driven by thermal heating of the rim slope. These winds are reinforced by the large-scale tidal wind patterns at this time [*Fenton and Richardson*, 2001; *Wilson and Hamilton*, 1996]. Such strong stresses may sustain local storms observed to propagate northward along the western rim of Hellas. Daytime slope-flow also develops on the northern and eastern rims. To the north, these winds may be responsible for sustained lifting toward the start of the global storm. To the east, these winds are opposed by the larger scale tidal flow, reducing the strength of the winds (not shown). To the south, daytime upslope flow out of the basin is strongly opposed, and overwhelmed by the low-level, off-cap winds, which flow toward and into the basin.

#### 4.2. High-Resolution Observations of Southern Hemisphere Seasonal Cap Edge Dust Storms and Dust Lifting in Hellas

[33] During the early period of dust activity in and near the Hellas basin, higher resolution (930 m/pixel) WA images were acquired with the red WA camera. Images from this collection exhibiting significant dust activity are shown in Figures 6a–6h. The images are all from the southern seasonal cap edge region or from within the Hellas basin. Unlike the DGM images, these higher resolution images were not continuously collected, but instead were targeted. As a result, these images are biased in their coverage compared to the DGMs. In Figures 6a–6h, the images have been map projected (polar stereographic) and cropped to highlight the dust activity. The images cover the period from $L_s = 171°$ to $L_s = 187°$, with eight of the nine images collected after the start of major activity ($L_s = 183°$) in Hellas.

[34] The first frame shows a diffuse dust cloud in the eastern portion of Hellas. The seasonal cap can be seen as the bright region in the lower right part of the frame. Such diffuse clouds are identified as dust by reference to the lower resolution color images. While many local storms were observed in the DGM images (see section 4.3), two factors resulted in very few storms being acquired in the higher resolution imaging. First, their transient nature makes them intrinsically hard to image; acquisition of storms in such targeted imaging is a sampling exercise and not guaranteed. Second, in comparison to the DGM images, the number of regional WA images was small and the coverage was limited.

[35] Figure 6b shows a more detailed view of the local storm evident in Figure 4g, which was located between the cap edge and the southwestern rim of Hellas. As argued in the previous section, the development and propagation into the Hellas basin of such cap edge storms likely contributed to the initiation of the larger dust storm event. Figure 6b shows significant, billowy structure and relief in the dust cloud top, suggesting convective activity. Similar morphological discussion was provided by *Briggs et al.* [1979] when studying dust storms with the Viking camera. While it is not possible to directly identify the direction of the mean wind in this image, the structure of the cloud may provide some information. On the southern side of the cloud, sharp individual fingers of dust were aligned normal to the cap edge (especially in the right hand portion of the dust cloud). Further north, these fingers combined and the cloud took on a thicker and more uniform, though still billowy character. It is possible to argue that the fingers represented individual dust lifting plumes, being blown to the north and combining to form the main cloud. This direction of flow would be consistent with the off-cap, low-level wind predicted by a thermally driven "sea-breeze" circulation at the cap margin [*Burk*, 1976; *Siili et al.*, 1997; *Toigo et al.*, 2002].

**Figure 5.** Output from a Mars MM5 mesoscale model [*Toigo et al.*, 2002] simulation of the southern hemisphere for $L_s = 180°$. The model initial and boundary conditions come from a global model simulation providing a good fit to air temperature and surface pressure observations. The model uses an interactive dust scheme as described by *Toigo et al.* [2002] (the observed TES dust is not prescribed). The polar cap edge was prescribed on the basis of MOC and TES observations. Each panel is a snapshot from the simulation, at 3-hour intervals (1 hour is defined here as 1/24th of a Martian day). The southern polar residual cap is located at the bottom of each frame at center. The latitude at upper center is roughly 20°S. Hellas appears to the right and Argyre appears to the left of each panel. The color shaded quantity for each panel is topography, with "warmer" colors signifying higher terrain and "cooler" temperatures signifying lower terrain. The model projection was polar stereographic. Temperatures are shown at 10 K intervals by green contours, providing information on the cap edge location and the surface thermal gradients. Stress is contoured in black at intervals of 0.01 Pa, starting at 0.02 Pa. White arrows for each model grid point represent the wind field. The indicated local time is for the domain central meridian of 30°E.
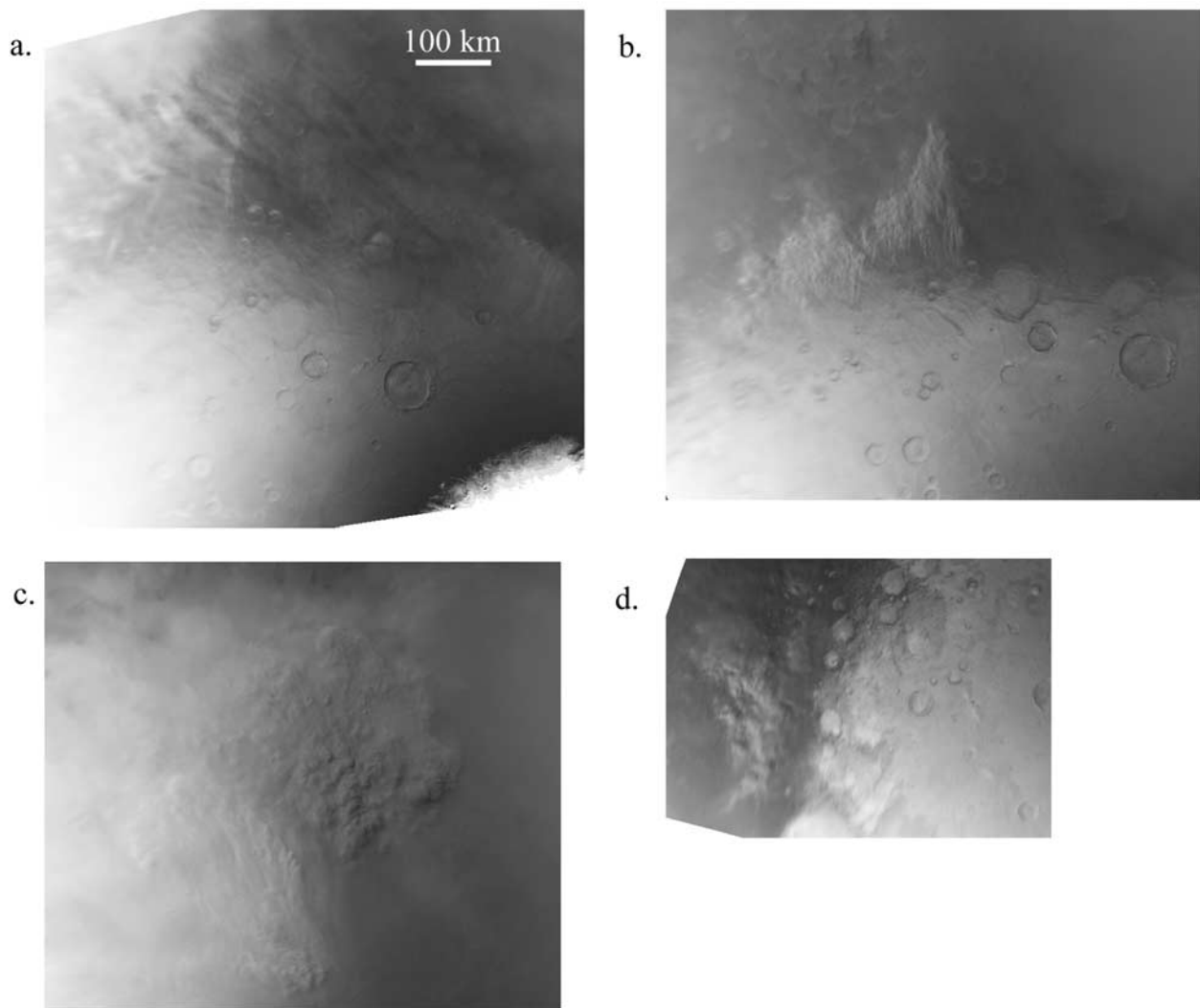
**Figure 6.** MOC regional wide-angle views of dust lifting events in the region around Hellas. All MOC images were radiometrically and photometrically corrected and map projected using the ISIS software package. North is up in all MOC image frames shown in this figure. Due to their proximity to the south pole, the wide-angle images presented in his figure are shown in polar projection. (a) Small early dust lifting activity at $L_s = 171°$ in eastern Hellas Planitia; (b) cap edge dust storm at $L_s = 182°$ near the southeast rim of Hellas Basin; (c) dust lifting center at $L_s = 183°$ in central Hellas Planitia; (d) cap edge dust storm at $L_s = 185°$ in Noachis Terra; (e) dust storm resembling convective clouds on Earth at $L_s = 185°$ in western Hellas Planitia; (f) more "convective type" dust lifting at $L_s = 187°$ in southern Promethei Terra; (g) growth of dust lifting center at $L_s = 187°$ along the southeast rim of Hellas Basin; (h) dust is blown out of the Hellas Basin, changing the dust activity from local to regional at $L_s = 187°$. A MOLA shaded relief map locating each MOC WA image (by panel letter) of this figure is provided for context between Figures 6g and 6h. The MOLA map has the south pole at the top and Hellas at the bottom.

Figures 6c–6e show additional isolated local dust storm activity in and around Hellas. All of the frames suggest vigorous stirring, and potentially lifting, of dust. Insofar as these images are representative of the seed events for the global storm, the images suggest a minimal role for dust devil activity in storm initiation, though the images are sufficiently low resolution that only the very largest dust devils observed anywhere on Mars by MOC [*Fisher et al.*, 2005] would be detectable.

[36] The final three images in Figures 6a–6h (Figures 6f, 6g, and 6h) show dust lifting during the dust storm's expansion out of Hellas. The three frames show dust clouds over Hellas and Promethei Terra, to the south and east of Hellas. In none of the three frames can dust lifting be directly observed, unlike the case with the local storm shown in Figure 6b (i.e., the authors cannot see any distinct indication of dust plumes, such as were evident in the latter frame). However, substantial clumping and billowing of the cloud tops can be seen, suggesting strong convective motions. Such cloud top relief can be seen in the DGM images, but in less detail. Later in the storm evolution, the dust loses such strong cloud top relief and billowing. Indeed
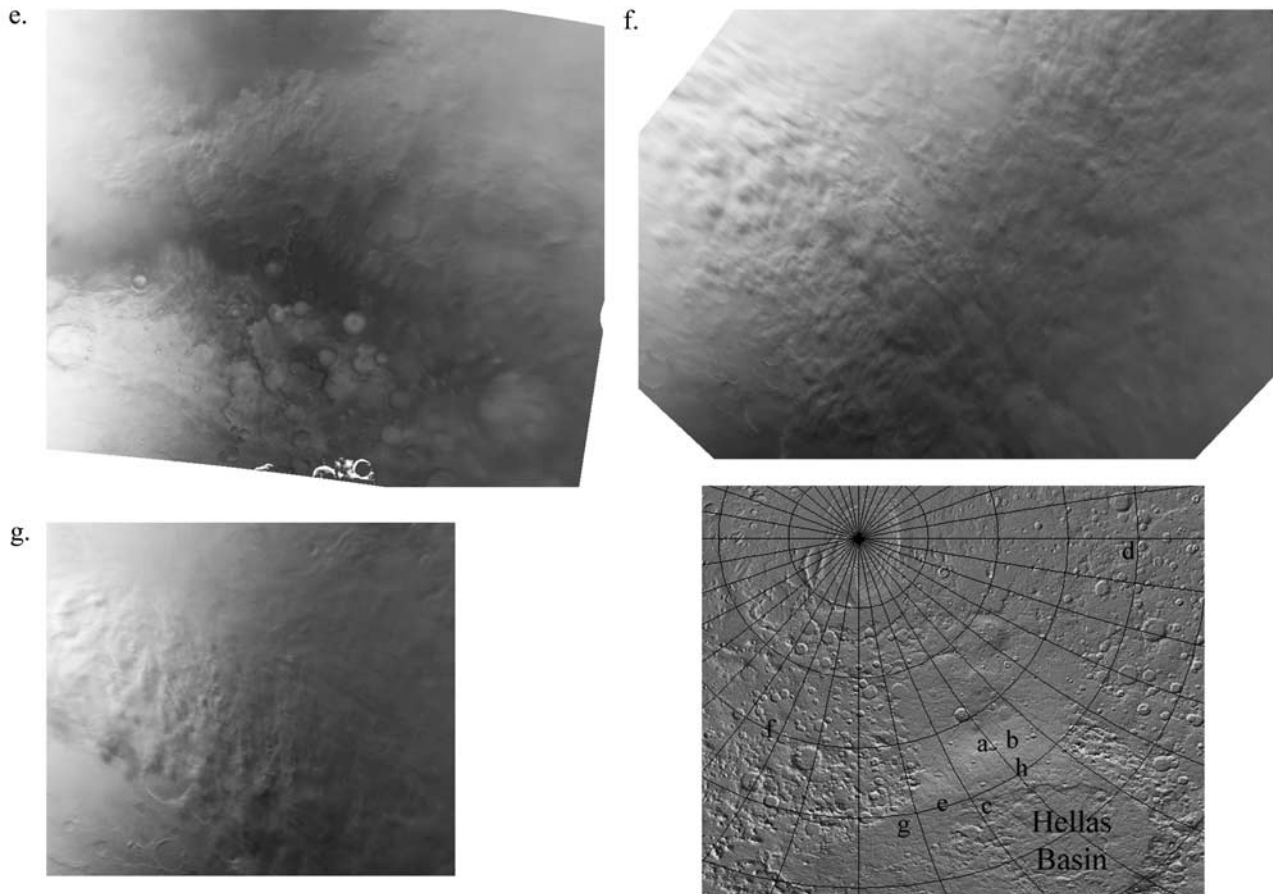
**Figure 6.** (continued)

in the full MOC WA frame sampled in Figure 6g (e0503566), a thick dust haze with very little cloud top structure extended to the north (up in the frame) and away from the active and turbulent zone shown in the image. An interpretation is that dust was being activity lifted in the "billowy" portion of the frame before being advected away to the north. All of the images show significant, crisp cloud-top structure; in the later frames especially, there is strong variation in the nature of this structure. Across Figure 6h, the scale and crispness of the "clumping" varies significantly, for example. Variation in the cloud top structure was observed during the large dust storms of 1977 by Viking [*Briggs et al.*, 1979], but in that case, the variation was ascribed to large differences in local time across the very wide field-of-view images. Variations in the dynamics of the dust cloud indicated in the Figures 6a–6h images must have more to do with significant variations in the nature of convective and mesoscale winds within the cloud deck.

[37] Figures 6f–6h offer an opportunity to measure the height of the dust cloud deck because the clouds cast visible shadows onto the surface. The illumination angle and image resolution are known, and if we assume a flat surface, the cloud deck height can be estimated. We made several measurements of the cloud heights in each frame, and the results are provided in Table 1. The average value in each case sits between about 5 and 8 km, which is roughly the estimated daytime mixed boundary layer height [*Gierasch and Goody*, 1968]. These measurements are thus consistent with the idea that dust is being lifted by boundary-layer turbulent processes and is mixed thoroughly within the boundary layer before it is transported to higher altitudes within the free atmosphere.

### 4.3. Comparison of Activity: 1999 Versus 2001

[38] MOC WA images show that the propagation of small storms from the southern seasonal $CO_2$ cap edge along the western rim of the Hellas basin is critical in the initiation phase of the 2001 global dust storm. Seasonal cap edge storms were observed frequently in the first MGS mapping year (data collected in 1999, in which there was not a full global dust storm) [*Cantor et al.*, 2001], and we have observed a significant number in the second mapping year, prior to the 2001 global storm. An important question for understanding triggering of the 2001 global storm therefore regards the relative activity of seasonal cap edge storms in 1999 and 2001. For example, if activity were greater in 2001 that may explain the triggering in of the global storm in that year rather than 1999, while generating a further question about why activity was greater in 2001.

[39] In order to address the question of seasonal cap edge storm activity, we counted the number of seasonal cap edge storms around the whole southern cap in each Martian day,
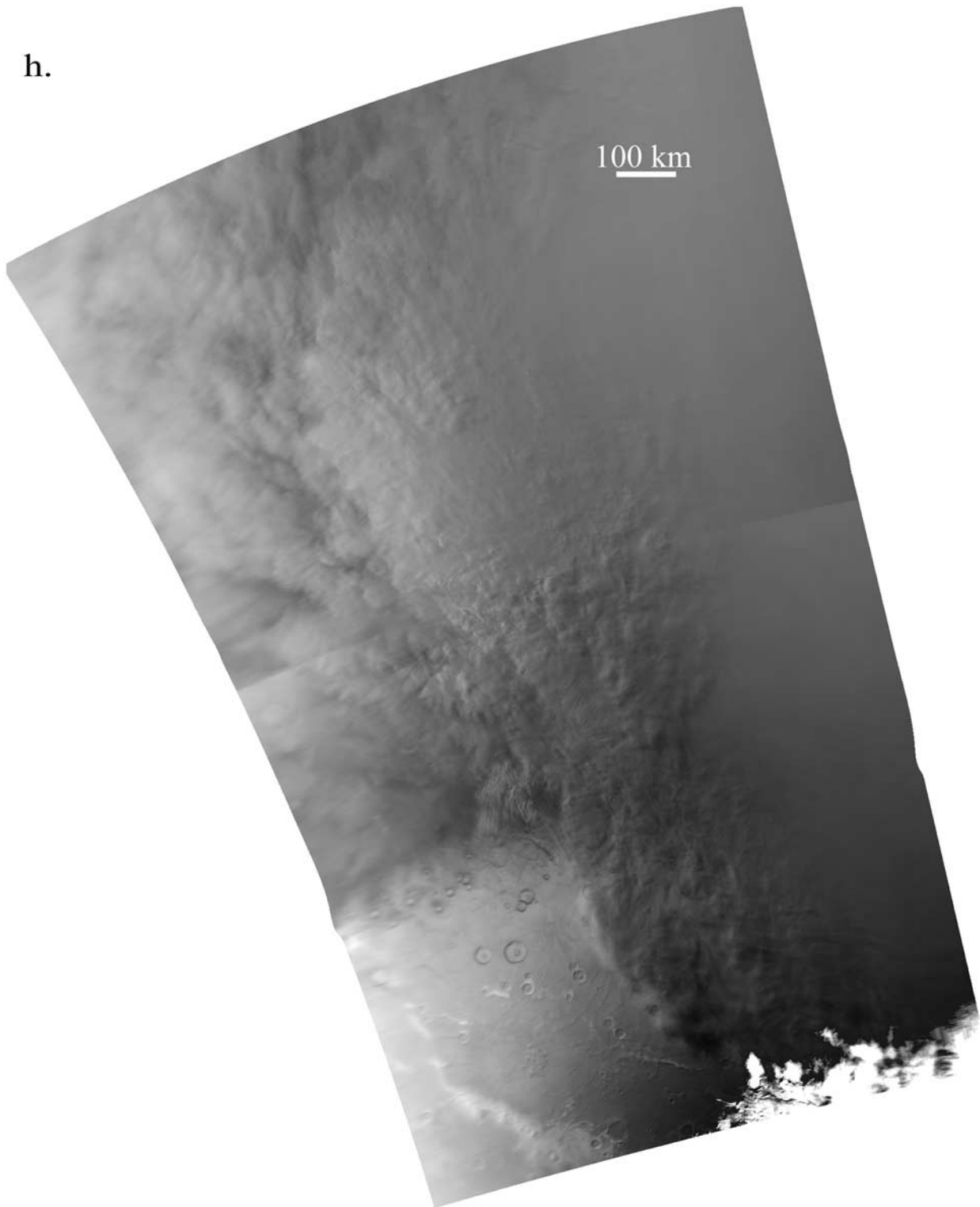
h.



100 km

**Figure 6.** (continued)

starting at $L_s = 170°$. This was about two weeks prior to the first indication of activity associated with the 2001 storm ($L_s = 177°-180°$). These data are shown in Figure 7a. Care was taken not to count storms more than once that appear in more than one DGM WA frame during a given day. Figure 7a does not show a great deal of difference in the number of storms between the two years. The only significant exception was the period between $L_s = 177°$ and $178°$,

**Table 1.** Estimates of the Height of the Dust Cloud Decks in the MOC WA Images Shown in Figures 6f–6h[a]

| e0503557 (Figure 6f) | e0503566 (Figure 6g) | e0503588 (Figure 6h) |
|---|---|---|
| 5.496 | 4.331 | 7.857 |
| 8.315 | 4.100 | 6.645 |
| 6.844 | 5.395 | 6.061 |
| 8.195 | 5.395 | 6.645 |
| 6.844 | 6.871 | |
| 8.195 | | |
| 6.844 | | |
| *7.248* | *5.218* | *6.802* |

[a]The estimates were obtained by measuring the length of the shadows cast by the clouds on the ground and using knowledge of the illumination angle and the assumption of a flat surface along with the pixel resolution to obtain the cloud deck height from Pythagoras's rule. The heights are given in kilometers, with the estimates shown in standard type, and the mean values indicated in italic bold type.

when a spike in the number of seasonal cap edge storms occurred in the second mapping year. Typically, $3 \pm 1$ southern cap edge dust storms were ongoing during any given day between $L_s = 170°$ and $184°$ in 1999 and 2001. During the two days between $L_s = 177.5°$ and $178°$, 7 and 9 distinct seasonal cap edge storms were raging. However, this spike in activity during these two days 2001 did not cause a noticeable increase in cap edge storm numbers during the $6°$ of $L_s$ that followed $L_s = 178$ in 2001 and preceding the global storm. It would thus be very difficult to argue that 2001 was any more active than 1999 only on the basis of the number of storms present.

[40] Figure 7b shows the combined area of southern seasonal cap edge dust storms during each day for the same period covered in Figure 7a. These areas were calculated in the same manner described by *Cantor et al.* [2001] (we used the same interactive IDL utility, DEFROI, for this purpose). The trend in storm area shows a somewhat different story regarding differences in cap-edge storm activity between the two years than that of storm number. Prior to $L_s = 177°$, the day-by-day total storm area was similar in both years with, if anything, a bias for a greater area of storms in 1999. That tendency ended sharply at $L_s = 177°$, when the number and total area of cap edge storms increased dramatically in 2001. Following this major spike, which corresponded near Hellas to the storm in Figure 4a, the area of seasonal cap edge storms was significantly higher than prior to $L_s = 177°$ in 2001. The mean area after $L_s = 177°$ in 2001 was twice that before, and was comparably larger than the mean area throughout the period $L_s = 170°–187°$ in 1999. The very pronounced activity of $L_s = 177.5°–178°$ in 2001 is something of a mystery. Roughly half of the cap edge storm activity (by area) occurred within the immediate vicinity of Hellas. The remainder took place in Sirenum (130°–145°W) and in Aonia (80°W). After the spike, the persistent doubling of storm area as compared to 1999 appeared to result from the maintenance of significant local storm activity in and around Hellas, in addition to the "normal" (as compared to 1999) generation of cap edge storms at a variety of other longitudes. The persistent action of local dust lifting within Hellas following the "seeding" event just after $L_s = 177°$ appears critical to the initiation of the 2001 global dust storm as indicated in the MOC DGM

images (Figures 4a–4m). This event is the most directly identifiable trigger for the initiation of the global storm.

## 5. Evolution of the 2001 Global Dust Storm
### 5.1. Storm Growth: From Hellas to the Edge of Tharsis

[41] The expansion of the storm out of the Hellas basin is illustrated in Figures 8a–8l, which shows portions of MOC DGM images (60°S and 60°N, and 40°E and 180°E) from 12 consecutive days spanning the period from $L_s = 182.7°$ and $188.9°$. During this period, dust was transported rapidly to the north, east, and to the south, such that by $L_s = 188.9°$, dust filled all longitudes between western Hellas and western Tharsis. The portion of this dust spreading that occurred over the southern polar cap is illustrated in Figure 3.

[42] At the beginning of the sequence ($L_s = 182.7°$), persistent dust activity was limited to the northwestern rim of Hellas. This image (Figure 8a) corresponds to a wider view of the DGM sampled in Figure 4h. Over the next 5 days ($L_s = 182.7°–185.5°$), dust expansion to the north and east of Hellas was evident. The images suggest that expansion involved the episodic "pumping" of dust initially to the north, into Syrtis, followed by eastward transport of these latitudinally extended dust clouds. Some care must be take in the identification of north-south running bands, however, as bands of "blurring" occur in the mosaicked images in this direction associated with emission angle variations across the individual WA images composing the DGM mosaic (dust opacity is emphasized in the high emission angle pixels).

[43] Progress of the expansion between Figures 8b and 8f was quite limited in comparison with the rapid expansion that ensues. Over the four days that separate Figures 8f and 8j ($L_s = 185.5°–187.8°$), a massive amount of dust spilled across Hesperia, covering about 40–60 degrees of longitude ($\sim$1200–1800 km). This corresponds to a mean transport rate of roughly $15–20$ ms$^{-1}$. The majority of this expansion was restricted to latitudes south of about 30°S. During this same period, northward expansion took place initially northward through Syrtis and Isidis to $\sim$45°N. Between Figures 8g and 8i ($L_s = 186°$ and $187.2°$) dust clouds with significant structure obscured the dark albedo Syrtis region. In the following two days (Figures 8j and 8k), much of the tropical and northern midlatitudes became obscured.

[44] The distinct cloud belts and structures visible in all of the images up to roughly $L_s = 187°$ began to blend into a more uniform dust haze in the final two panels of Figures 8a–8l. While some variation in the dust haze can clearly be seen in Figure 8l, the surface can only been seen in the extreme northwest of the frame. The latitudinal gradient of opacity that is so evident in Figures 8h–8j essentially disappeared by Figure 8l.

[45] Some of the structure seen in Figures 8k and 8l in the northern high latitudes is quite interesting. In the northeastern and northwestern portions of Figures 8k and 8l are concentrated dust belts which appear quite similar in shape to dust belts observed to develop in the equinoctial northern midlatitudes in the absence of high global dust opacities [*Cantor et al.*, 2001; *Wang et al.*, 2003]. These belts are likely associated with low-pressure frontal cyclones [*Wang et al.*, 2003], and their presence in Figures 8k and 8l
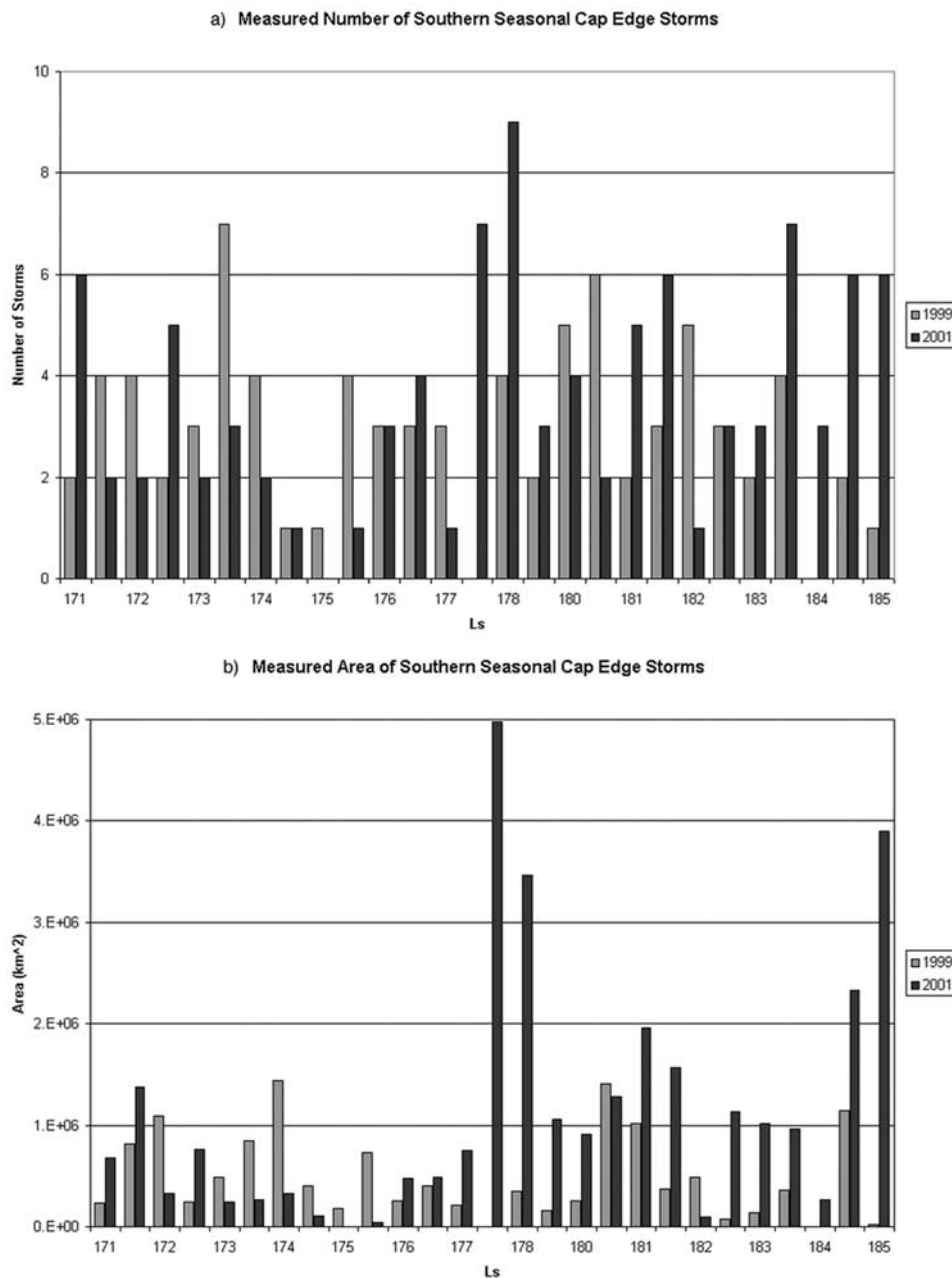
a)  Measured Number of Southern Seasonal Cap Edge Storms



b)  Measured Area of Southern Seasonal Cap Edge Storms



**Figure 7.** Comparison of storm activity between 1999 and 2001. Number of seasonal cap edge storms for each year is shown in Figure 7a, while the area of the planet enshrouded by dust storms in each year is shown in Figure 7b. 2001 does not appear much more "active" than 1999 in the early stages of storm development. The first indication of increased dust lifting in 2001 comes at $L_s = 178°$, when sharp increases are visible in the number and area of storms.

probably results from the concentration of dust haze associated with the incipient global dust storm by convergent winds in the cyclone fontal zone.

[46]  In summary, dust spread out of the Hellas basin and filled the fraction of the planet between Hellas and Tharsis in a period that was comparable to that during which dust activity built in and around Hellas (~6 days in both cases). Dust initially spread to the east in the southern mid- and high-latitudes, with a strong meridional dust opacity gradient developing. This gradient persisted for a very short period (~4 days) being subsequently and rapidly wiped

out as dust filled the tropics and northern high latitudes. While the expansion proceeded to the east, no expansion occurred to the west. This is a significant aspect of the storm that will need to be explained by any model of storm growth.

## 5.2.  Syria/Solis and Daedalia Secondary Dust Lifting Centers and Global Expansion

[47]  The final stage of evolution of the 2001 global storm is shown in Figure 9. Full DGM equatorial maps (60°S– 60°N and 180°W–180°E) are shown for five time steps

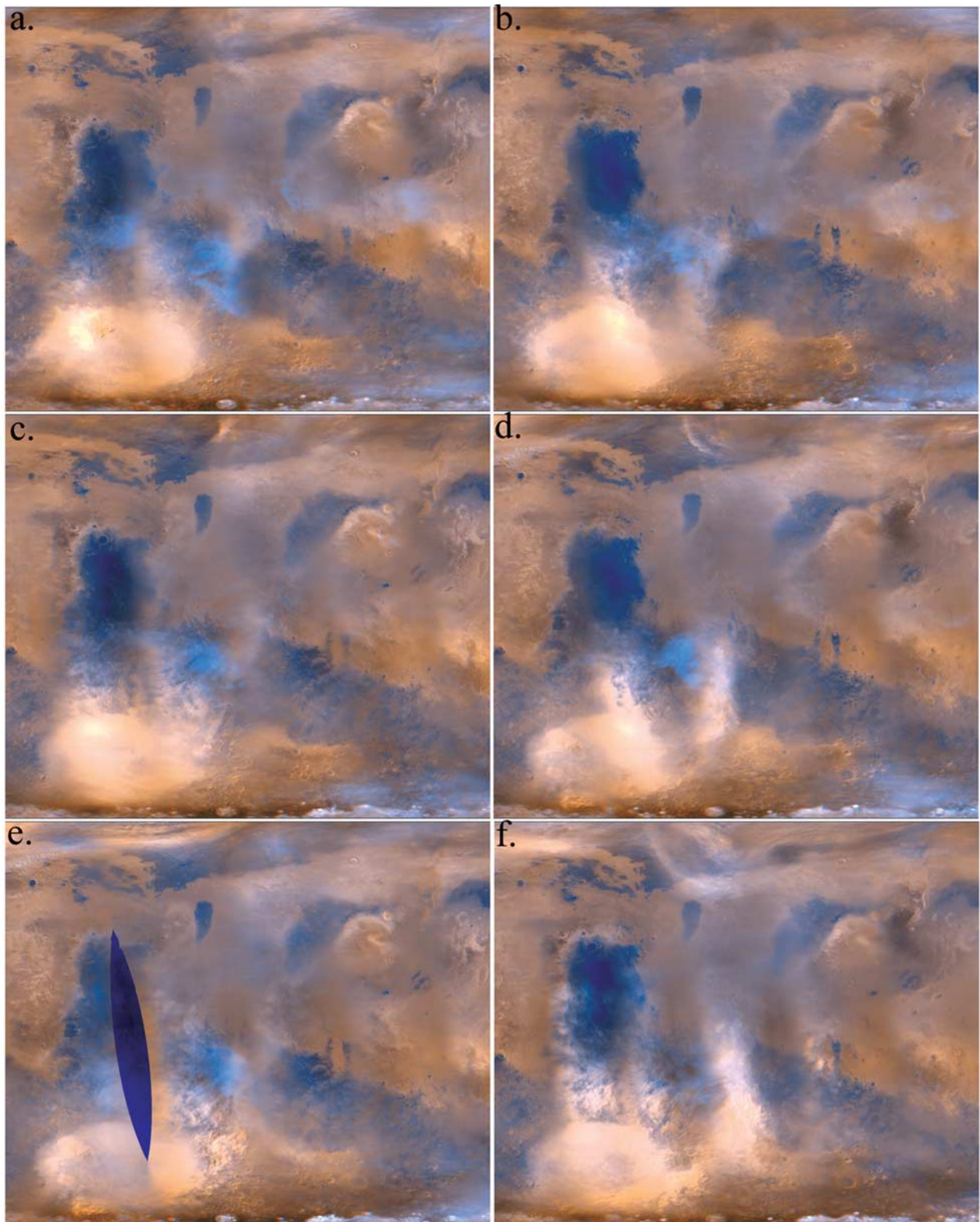**Figure 8.** MOC DGM mosaics showing 60°S to 60°N, 40°E to 180°E between $L_s = 182.7°$ and $L_s = 188.9°$. The progression in these frames shows (a–f) the growth of the dust lifting center in the Hellas region with gradual diffusion of dust slightly to the east from Hellas, (g–j) subsequent rapid spreading of dust north and east from Hellas, and finally (k and l) obscuration of the surface between Hellas and the Tharsis ridge.
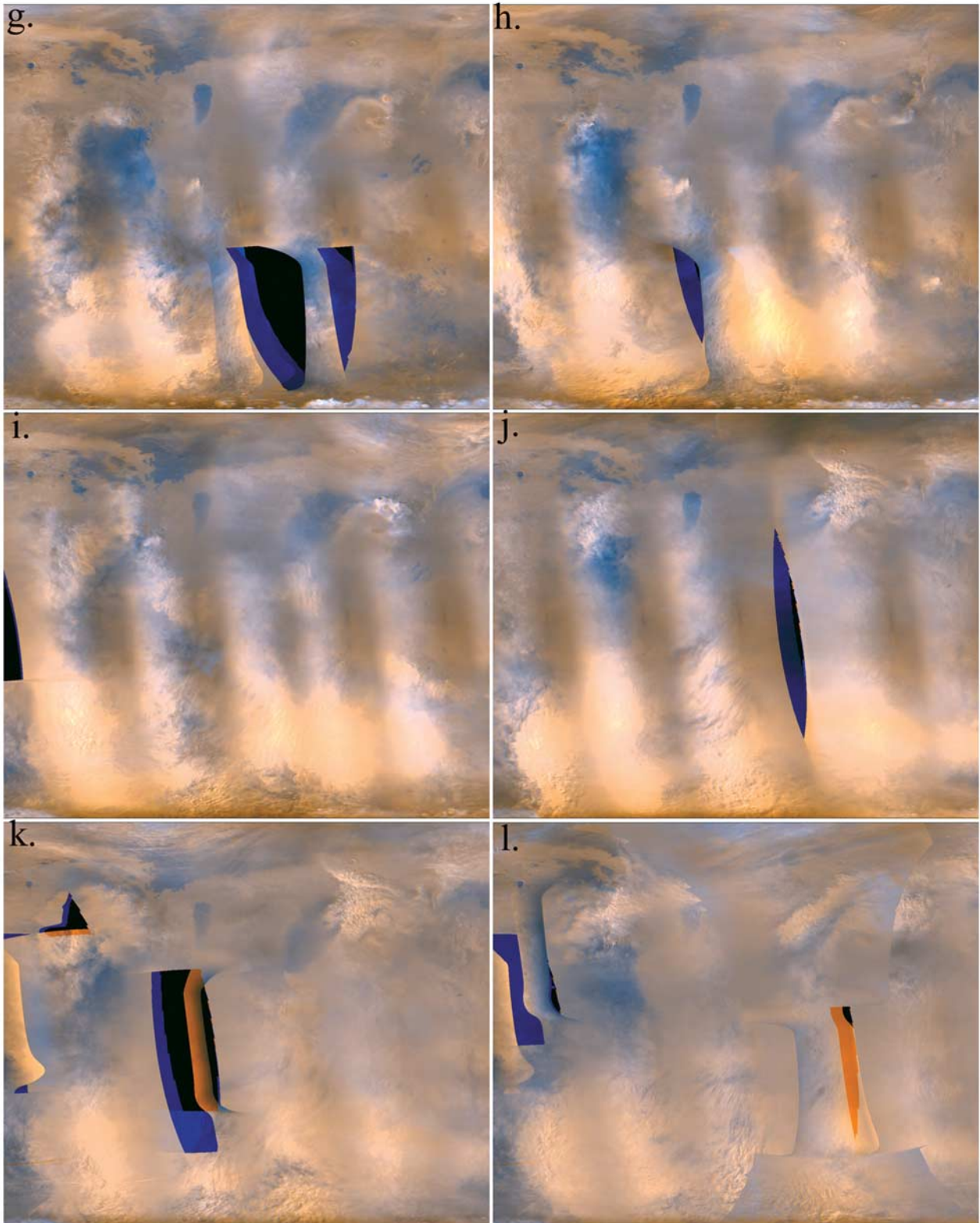
**Figure 8.** (continued)

separated by two days each between $L_s = 188.9°$ and $193.5°$. The first frame includes the image shown in Figure 8l. At this time, dust extended in a thick haze from western Hellas to the western slopes of Tharsis but a substantial portion of the planet to the east of Tharsis was still relatively clear, with detailed surface features remaining evident, including the Argyre basin, Valles Marineris, and the low albedo regions of Acidalia and Margaritifer.
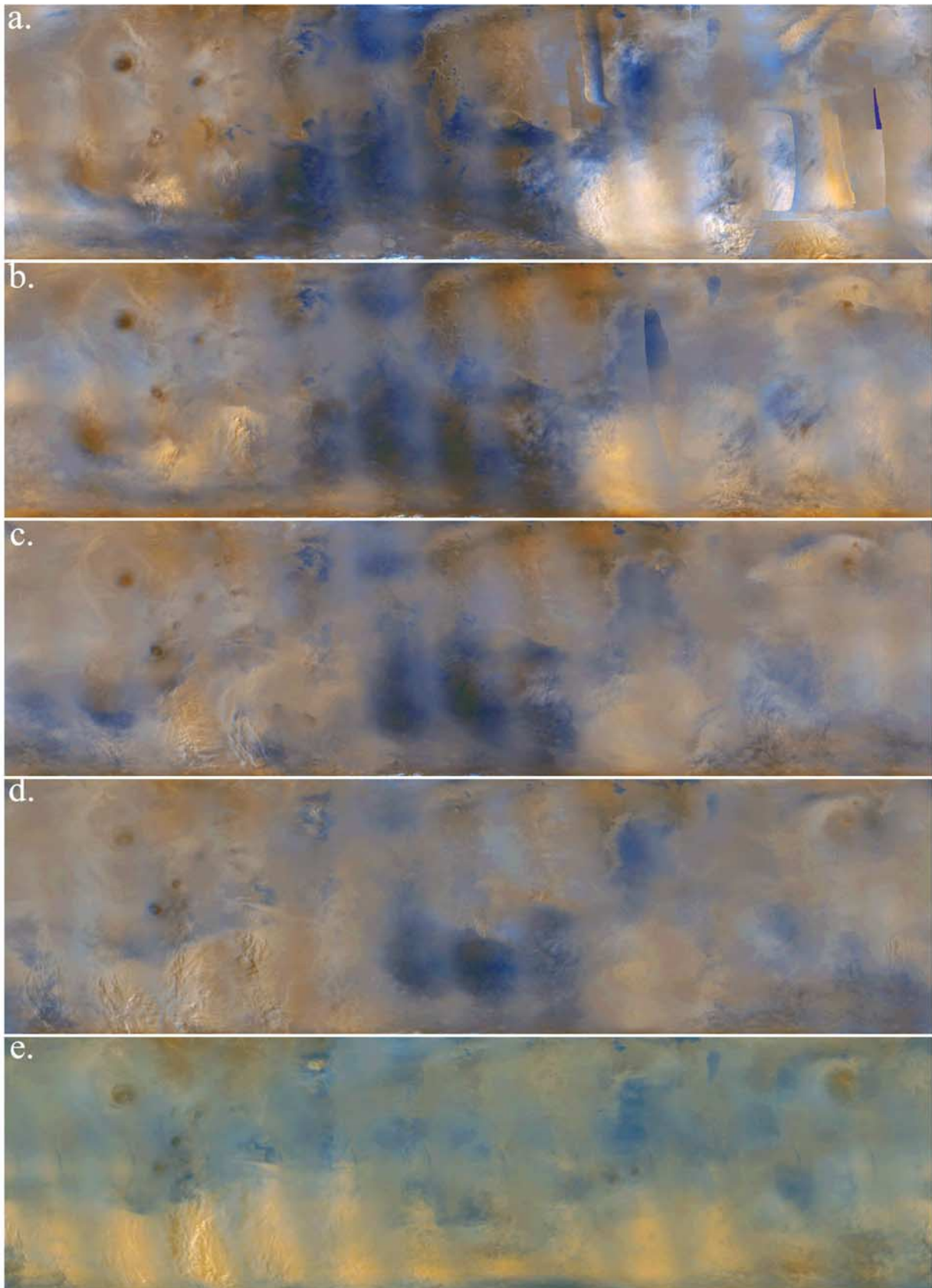
**Figure 9.** MOC DGM global mosaics showing 60°S to 60°N for $L_s$ = 188.9° to 193.5°. These images show the progression of the 2001 storm from a series of independent regional dust storms to a planet-enshrouding global dust storm. This transition occurs largely over only 5° of $L_s$.
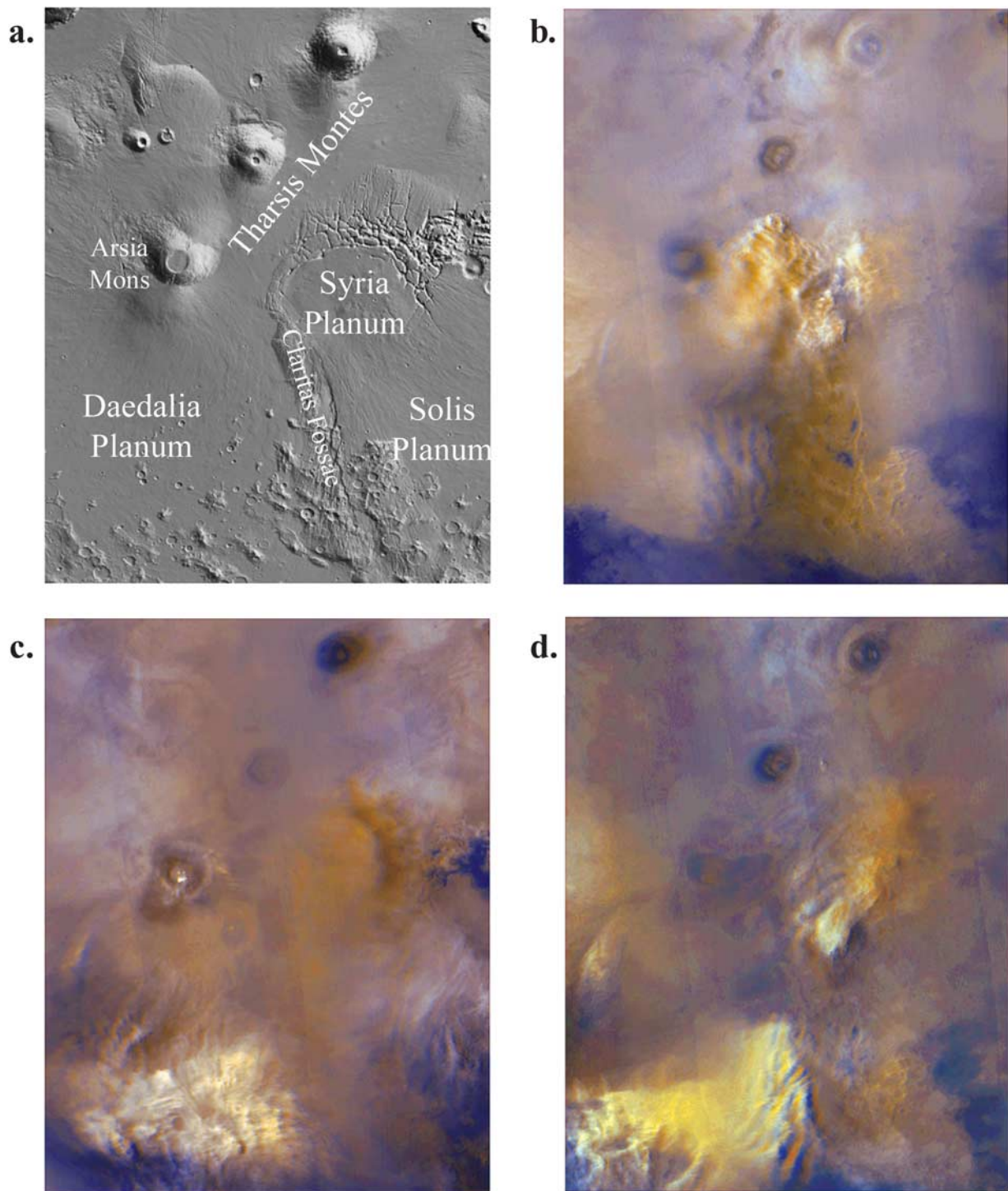
**Figure 10.** The initiation and initial evolution of the secondary dust lifting centers in the Syria/Solis/Daedalia region. Each frame covers the same geographical subsection of MOC DGM global mosaics, from 20°S to 10°N, 235°E to 270°E. (a) MOLA topography for reference; (b) $L_s = 188.3°$; (c) $L_s = 188.9°$; (d) $L_s = 189.5°$.

[48] Prior to $L_s = 188.9°$, no significant dust lifting occurred over or to the east of Tharsis. However, at this time, two distinct secondary dust lifting centers became active in the Daedalia, Syria, and Solis regions south of the Tharsis shield volcanoes. Figure 10b shows the first lifting on the eastern side of Tharsis, in Syria and along the northern part of the Claritas ridge. Enhanced dust persisted in this location for the next two days shown in

**Figure 11.** This summary figure shows a MOC DGM global mosaic overlain by orange layers of varying opacity indicating the time of dust coverage. The t = 0 corresponds to $L_s$ = 180, with each consecutive contour indicating 5 Martian days of storm development (i.e., t = 10 corresponds to 10 Martian days after the first contour). The more opaque areas (like those over the Hellas region) became obscured by dust earliest; the areas overlain by more transparent orange layers became covered in dust later in the storm's growth. It is clear that the storm originated over Hellas and spread north and west. At the same time as spreading dust from Hellas was arriving at the western edge of the Tharsis ridge, separate dust lifting centers were developing on the eastern edge of the ridge, over Syria/Solis and Daedalia. Eventually, dust from both the primary and secondary lifting centers filled the remaining clear atmosphere as the storm became a truly global phenomenon. The figure was made by examination of MOC DGM global mosaics and subjectively contouring the "edge" of the storm. Comparison with Figure 2 suggests that this edge corresponds to an infrared opacity of about 0.5 to 0.75.

Figures 10c (also 9a) and 10d, as an additional center in Daedalia became active. Over the next four days these two centers merged into a single system, separable from the increasing background haze by their substantially elevated optical depth, crisp definition, and fine, "billowy" cloud top structure, which combines to suggest active lifting. While Solis and the Claritas ridge have been associated with dust lifting at the initiation of previous global dust storms, and specifically the 1977a storm [*Briggs et al.*, 1979], it has occurred to the authors and independently to one of our reviewers (P. James, personal communication, 2004), that the sparse sampling of the 1977a storm by Viking does not rule out an origin similar to that of the 2001 storm. At $L_s = 194°$, Viking images show dust clouds in western Hellas similar to those observed by MOC. The Viking Infrared Thermal Mapper (IRTM) retrievals at this time showed high opacity in Hellas [*Martin and Richardson*, 1993]. Observations to the east of Hellas for the period between the Hellas event and the Solis event in 1977 are poor, with no coverage of Hellas for the maps corresponding to $L_s = 200°-215°$. The data between Hellas and Tharsis that do exist between $L_s = 190°$ and $205°$ do not provide compelling evidence for a 2001-like storm evolution; indeed, they show something of an opacity minimum, but the data are ambiguous due to coverage. Probably all that can be said is that in 1977, strong dust activity in Hellas from just before to just after equinox was followed by activation of lifting in Solis, followed by expansion to a global storm and in that respect 2001 and 1977a were similar.

[49] The region between Tharsis and Hellas, by way of the prime meridian, became increasingly hazy during the period documented in the first three frames of Figure 9 (up to $L_s = 191°$). However, the region was not overrun by dust clouds advancing from either Tharsis or Hellas, but rather became dustier due to the steadily accumulating diffuse haze during this interval. This was presumably accomplished by steady "leakage" of dust into the free atmosphere from the boundary layer in regions of thick dust, followed by diffusive transport of the dust to the rest of the planet by the large scale circulation. The rapidly building dust cloud in Syria and Solis may have been the primary source of this dust due to its proximity, the coincidence of timing between the rising haze opacity just after the initiation of the Syria/Solis/Daedalia lifting center, and the observation of eastward (westerly) transport of dust that characterizes all of the dust transport during the growth of the 2001 global storm. (The authors note that when the DGMs are viewed as frames in a movie, the primary fluid motions noticed are "wafting" of dust to the north from lifting centers in the south, followed by advection to the east. The impression is that of smoke rising and diffusing, and then advecting to the east in response to a lateral wind). Additional contribution to the rise in the dust haze likely came by way of the high northern latitude westerlies. The DGM mosaics show opacity increasing north of Tharsis and spreading of this dust to the east during this period. Given that significant dust appears to have been transported into the high northern latitudes north of Elysium (Figure 8l), it would seem hard to imagine how this dust would not get rapidly

transported to the east by the near-surface expression of the winter polar jet.

[50] By $L_s = 193.5°$ the storm had reached a fully global state. Very few surface features, with the exception of the tallest volcanoes can be identified in images from this time. Evident in Figure 9d and 9e, is the fact that the Syria/Solis/Daedalia lifting center (which now extended southward into Sirenum, Aonia, and Argyre) became much more pronounced than the Hellas center. Indeed, by this time Hellas appeared to have become covered in the same quiescent, thick haze as much of the rest of the planet. Although it is not possible to make definite statements about the termination of dust lifting in Hellas (because it is possible that dust lifting there became hidden by overlaying haze), the general impression of lower opacity in Hellas versus the extended Syria/Solis/Daedalia center, and the apparent ability to identify the geographical shape of the Hellas basin suggests that dust lifting was substantially less vigorous there at $L_s = 192°$ (Figure 9d and thereafter) than only a few days early at $L_s = 188.9°$ (Figure 9a). On the basis of these observations, we would estimate that substantial dust lifting in Hellas terminated around $L_s = 191°$, and that thereafter, the Syria/Solis/Daedalia center dominated dust supply. If this is correct, it is unclear why the Hellas center shut off at this point. Possibilities include exhaustion of available surface dust, changes in the global circulation as the dust became more uniform that weakened winds in Hellas, and radiative-dynamical feedback associated with shading of the surface by the thickening atmospheric dust haze. The latter seems unlikely in our view as dust lifting persisted and grew in Hellas for at least 8 days prior to $\sim L_s = 190°$ during which time the opacity in and around Hellas was higher than that during the period following $L_s = 190°$.

[51] In summary, the rapid eastward transport of dust from the Hellas basin illustrated in Figures 8a–8l was apparently blocked by the Tharsis plateau. Instead of continued transport, the storm developed from this point through the activation of secondary dust lifting centers to the southeast of the Tharsis ridge shield volcanoes (Syria/Solis). These lifting centers rapidly combined, and by $L_s = 190°$ appeared to have taken over as the primary dust lifting center in the storm. Haze built in the region that had not been previously consumed by dust transport from Hellas, likely by transport of dust from this secondary center. By $L_s = 193°$ the storm had become fully global. The transition from a Hellas basin storm to a hemispheric storm, and then the transition from hemispheric to fully global storm each took about 8 Martian days. Thus, in just a little over two Martian weeks, the Hellas basin regional storm had consumed the planet.

## 5.3. Storm Switch-Off

[52] The evolution of dust optical depth can be quantified from the TES thermal spectra and suggests that the storm obtained peak opacities around $L_s = 210°$ [*Smith et al.*, 2002]. From the perspective of infrared optical depth, the storm was in decay from this date. The MOC DGM images provide an independent means of assessing storm "switch-off" in terms of the termination of cloud-top morphological evidence for active dust lifting. Again, we

take billowy, clumpy cloud top structure to be such evidence. Examination of the MOC DGM mosaics following those shown in Figure 9 demonstrates that the Syria/Solis/Daedalia lifting center persisted as an active lifting site for a long time. As time progressed, the lifting center became smaller and retreated to its original position centered between Syria and Daedalia. The final frame in which cloud top structure indicative of active lifting can be seen is the eighth day of MOC observing phase E07 (corresponding to $L_s = 210.5°$), although sporadic re-emergence of structure occurred over the following week or so. As such we estimate the termination of active lifting associated with the 2001 storm at between $L_s = 210°$ and $214°$. This is in remarkable agreement with the "turn-around point" seasonal date for global dust opacity, and provides a direct illustration of the link between observable dust lifting and the trend of global dust. It also provides confidence in the use of cloud top morphology as an indicator of active dust lifting.

## 6. Summary

[53] The evolution of the 2001 global dust storm is summarized in Figure 11, which shows the geographical extent of the global storm at intervals of 5 Martian days from $L_s = 180°$ until the storm attained global extent. Figure 11 has been designed for easy comparison with the figure summarizing the 1973 storm produced by *Martin* [1973] and the 1977b storm produced by *Thorpe* [1979]. The latter has been reproduced by *Kahn et al.* [1992] as their Figure 2.

[54] The global storm began along the northwestern rim of the Hellas basin just before southern spring solstice. The storm was initiated as several local dust storms propagated into Hellas from the seasonal ice cap edge to the south. Seasonal cap edge dust storm activity prior to $L_s = 177°$ was little different in 2001 to that in the previous Martian year. However, between $L_s = 177°$ and $178°$, the area of local cap edge storm activity dramatically increased over that of the previous year, with this increase due almost completely to increased activity in the vicinity of Hellas, with area of lofted dust exceeding that in 1999 by over a factor of two thereafter.

[55] The early phase of the dust storm in Hellas was captured in detail in MOC WA images with resolution as high as 930 m/pixel. These images provide direct evidence of dust lifting in plumes at the edge of the dust storm. There was no evidence for involvement of dust devils. The dust is lifted to heights of $5-7.5$ km, about the height of the well-mixed daytime boundary layer top, at the periphery of the dust storm. As the measurements required observable shadows cast onto the ground, cloud deck altitude measurements deeper into the cloud we not possible. Observations of the well-developed 1971 and 1977 storms suggest dust haze deck elevations can reach up to 70km [*Anderson and Leovy*, 1978; *Jaquin et al.*, 1986]. The high-resolution WA images show a great deal of structure in the dust deck top early in storm evolution and significant spatial variability to this structure. Motions on scales as small as a few kilometers are indicated, while the heterogeneity suggests large variations in the vigor of mixing on scales of tens to hundreds of kilometers.

[56] Expansion of the storm out of the Hellas basin initially occurred to the north and to the east. No sustained transport to the west was observed, although "pulses" of dust to the west were (these pulses of dust are not readily apparent in individual frames, but are readily apparent when the frames are viewed as a movie). For five days following $L_s = 182°$, the storm persisted as a regional event spilling north and east of Hellas, but without significant net growth. After $L_s = 185°$, the dust storm rapidly broke out of the Hellas region, with large amounts of dust spilling across Hesperia. The highly asymmetric dust spreading, to the east and not to the west, does not appear to be a ready consequence of winds predicted by numerical models, which do not show such mono-directionality. (One should be careful in this regard: model diurnal mean winds at this season to the north of Hellas are to the east as part of the tropical jet [e.g., *Fenton and Richardson*, 2001], but rotate completely during the diurnal cycle as shown in Figure 5. An initial GCM study of dust storm evolution resulting from a source in Hellas, but at a somewhat later season, shows transport in both eastward and westward directions, which is contrary to observations [*Basu et al.*, 2004].) At the same time as the eastward expansion, dust began spreading to the south, across the southern cap.

[57] The main dust cloud reached the edge of Tharsis just before $L_s = 190°$. At this point, distinct secondary dust lifting events occurred on the Tharsis plateau to the south of the ridge volcanoes, in Solis/Syria and Daedalia. Three degrees of $L_s$ after the activation of the Solis/Syria/Daedalia lifting center, the storm had become fully global. If dust lifting is gauged by cloud top morphology, then lifting continued to be predominantly in the southern hemisphere throughout the storm growth. Prior to $L_s = 190°$, the majority of lifting was indicated in the Hellas region, after this date, the Syria/Solis/Daedalia center predominated. The Hellas center apparently shut-off just after Ls = 190°, while the Syria/Solis/Daedalia center remained active until roughly $L_s = 210°-214°$. This date coincides with the transition from opacity growth to opacity decay, as gauged from TES data.

[58] The 2001 Martian global dust storm provided the first opportunity of its kind: the study of another planet's extreme weather phenomena using multiple sets of high spatial and temporal resolution data. The thermal and photographic data from MGS TES and MOC instruments allow the recreation of the initiation and development of this storm. Five issues were highlighted at the end of Part 3, with which we conclude this study:

[59] 1. The propagation of cap edge dust storms into the Hellas basin appears to have been the initial trigger for the global storm. Southern cap edge storms were no more numerous near equinox in 2001 than in 1999 prior to the global storm, but a very large cap edge storm near Hellas at $L_s = 177°$ appears to have played the key role in separating the behavior in 2001 from that in 1999.

[60] 2. The storm grew in Hellas along the western and southern rims, consistent with model predicted regions of maximum wind stresses due to the combination of cap edge thermal contrasts, topographic slope flow, and the large-scale thermal tidal circulation.

[61] 3. Dust was transported out of Hellas to the east and not to the west. This mono-directionality is not understood

and would not be expected on the basis of numerical model wind predictions. The mean dust front migration, at a rate of about $15-20$ ms$^{-1}$, may correspond to dynamical induction of lifting or transport of dust from Hellas.

[62] 4. The activation of a secondary dust lifting center in Syria/Solis/Daedalia appears to have been important for the full global development of the storm and for the peak opacities obtained by the storm. This region is known for its historical involvement in large dust storms. It is possible that it was activated by enhanced Hadley circulation associated with the increased atmospheric dust opacity. Activation of secondary dust lifting in this region has been predicted with global numerical models [*Basu et al.*, 2004].

[63] 5. The Hellas basin appears to have terminated as a lifting site ($\sim L_s = 190°$) well before the Syria/Solis/Daedalia termination ($L_s = 210-214°$) marked the turning-point of the storm. It is not known why either lifting center terminated when they did. There was no major increase in opacity prior to switch-off that would suggest a radiative dynamical feedback. Changes in the circulation as the dust became more evenly spread on a global basis or the depletion of dust may explain the termination of both lifting centers.

## References

Albee, A. L. (2000), Mars 2000, *Annu. Rev. Earth Planet. Sci.*, *28*, 281–304.

Anderson, E., and C. Leovy (1978), Mariner-9 television limb observations of dust and ice hazes on Mars, *J. Atmos. Sci.*, *35*(4), 723–734.

Basu, S., M. I. Richardson, and R. J. Wilson (2004), Simulation of the Martian dust cycle with the GFDL Mars GCM, *J. Geophys. Res.*, *109*, E11006, doi:10.1029/2004JE002243.

Briggs, G. A., W. A. Baum, and J. Barnes (1979), Viking Orbiter imaging observations of dust in the Martian atmosphere, *J. Geophys. Res.*, *84*(B6), 2795–2820.

Burk, S. D. (1976), Diurnal winds near Martian polar caps, *J. Atmos. Sci.*, *33*(6), 923–939.

Cantor, B. A., and M. C. Malin (2003), Mars Orbiter Camera meteorological observations, paper presented at Mars Atmosphere Modelling and Observations, Cent. Natl. d'Etudes Spatiales, Granada, Spain.

Cantor, B. A., P. B. James, M. Caplinger, and M. J. Wolff (2001), Martian dust storms: 1999 Mars Orbiter Camera observations, *J. Geophys. Res.*, *106*(E10), 23,653–23,687.

Cantor, B., M. Malin, and K. S. Edgett (2002), Multiyear Mars Orbiter Camera (MOC) observations of repeated Martian weather phenomena during the northern summer season, *J. Geophys. Res.*, *107*(E3), 5014, doi:10.1029/2001JE001588.

Caplinger, M. A., and M. C. Malin (2001), Mars Orbiter Camera geodesy campaign, *J. Geophys. Res.*, *106*(E10), 23,595–23,606.

Christensen, P. R., et al. (1992), Thermal Emission Spectrometer Experiment: Mars Observer Mission, *J. Geophys. Res.*, *97*(E5), 7719–7734.

Christensen, P. R., et al. (2001), Mars Global Surveyor Thermal Emission Spectrometer experiment: Investigation description and surface science results, *J. Geophys. Res.*, *106*(E10), 23,823–23,871.

Conrath, B. J. (1975), Thermal structure of Martian atmosphere during dissipation of dust storm of 1971, *Icarus*, *24*(1), 36–46.

Conrath, B. J., J. C. Pearl, M. D. Smith, W. C. Maguire, P. R. Christensen, S. Dason, and M. S. Kaelberer (2000), Mars Global Surveyor Thermal Emission Spectrometer (TES) observations: Atmospheric temperatures during aerobraking and science phasing, *J. Geophys. Res.*, *105*(E4), 9509–9519.

Fenton, L. K., and M. I. Richardson (2001), Martian surface winds: Insensitivity to orbital changes and implications for aeolian processes, *J. Geophys. Res.*, *106*(E12), 32,885–32,902.

Fenton, L. K., J. C. Pearl, and T. Z. Martin (1997), Mapping Mariner 9 dust opacities, *Icarus*, *130*(1), 115–124.

Fernandez, W. (1997), Martian dust storms: A review, *Earth Moon Planets*, *77*(1), 19–46.

Fisher, J. A., M. I. Richardson, C. E. Newman, M. A. Szwast, C. Graf, S. Basu, S. P. Ewald, A. D. Toigo, and R. J. Wilson (2005), A survey of Martian dust devil activity using Mars Global Surveyor Mars Orbiter Camera images, *J. Geophys. Res.*, doi:10.1029/2003JE002165, in press.

Gierasch, P., and R. Goody (1968), A study of thermal and dynamical structure of Martian lower atmosphere, *Planet. Space Sci.*, *16*(5), 615–636.

Gierasch, P. J., and R. M. Goody (1973), Model of a Martian great dust storm, *J. Atmos. Sci.*, *30*(2), 169–179.

Greeley, R. (1992), Global stratigraphy, in *Mars*, edited by H. H. Kieffer et al., pp. 730–766, Univ. of Ariz. Press, Tucson.

Haberle, R. M., C. B. Leovy, and J. B. Pollack (1979), A numerical model of the Martian polar cap winds, *Icarus*, *39*(2), 151–183.

Haberle, R. M., C. B. Leovy, and J. B. Pollack (1982), Some effects of global dust storms on the atmospheric circulation of Mars, *Icarus*, *50*(2–3), 322–367.

Hanel, R., et al. (1972), Investigation of the Martian environment by infrared spectroscopy on Mariner 9, *Icarus*, *17*(2), 423–442.

Jakosky, B. M., and T. Z. Martin (1987), Mars: North polar atmospheric warming during dust storms, *Icarus*, *72*(3), 528–534.

James, P. B., R. T. Clancy, S. W. Lee, L. J. Martin, R. B. Singer, E. Smith, R. A. Kahn, and R. W. Zurek (1994), Monitoring Mars with the Hubble Space Telescope: 1990–1991 observations, *Icarus*, *109*(1), 79–101.

Jaquin, F., P. Gierasch, and R. Kahn (1986), The vertical structure of limb hazes in the Martian atmosphere, *Icarus*, *68*(3), 442–461.

Kahn, R. A., T. Z. Martin, R. W. Zurek, and S. W. Lee (1992), The Martian dust cycle, in *Mars*, edited by H. H. Kieffer et al., pp. 1017–1053, Univ. of Ariz. Press, Tucson.

Leovy, C. B. (1972), Generation of strong winds on Mars, *Eos Trans. AGU*, *53*(4), 460.

Leovy, C. B. (1985), The general circulation of Mars: Models and observations, *Adv. Geophys.*, *28*, 327–346.

Leovy, C. B., R. W. Zurek, and J. B. Pollack (1973), Mechanisms for Mars dust storms, *J. Atmos. Sci.*, *30*(5), 749–762.

Liu, J., M. I. Richardson, and R. J. Wilson (2003), An assessment of the global, seasonal, and interannual spacecraft record of Martian climate in the thermal infrared, *J. Geophys. Res.*, *108*(E8), 5089, doi:10.1029/2002JE001921.

Magalhaes, J. A., and R. E. Young (1995), Downslope windstorms in the lee of ridges on Mars, *Icarus*, *113*(2), 277–294.

Malin, M. C. (1992), Mass movements on Venus: Preliminary results from Magellan cycle 1 observations, *J. Geophys. Res.*, *97*(E10), 16,337–16,352.

Malin, M. C., and B. Cantor (2003), Mars Orbiter Camera climate observations, paper presented at Mars Atmosphere Modelling and Observations, Cent. Natl. d'Etudes Spatiales, Granada, Spain.

Malin, M. C., and K. S. Edgett (2001), Mars Global Surveyor Mars Orbiter Camera: Interplanetary cruise through primary mission, *J. Geophys. Res.*, *106*(E10), 23,429–23,570.

Martin, L. J. (1973), 1973 dust storm on Mars: Maps from hourly photographs, *Icarus*, *23*, 363–380.

Martin, L. J., and R. W. Zurek (1993), An analysis of the history of dust activity on Mars, *J. Geophys. Res.*, *98*(E2), 3221–3246.

Martin, T. Z. (1986), Thermal infrared opacity of the Mars atmosphere, *Icarus*, *66*(1), 2–21.

Martin, T. Z., and H. H. Kieffer (1979), Thermal infrared properties of the Martian atmosphere 2.15-μM band measurements, *J. Geophys. Res.*, *84*(B6), 2843–2852.

Martin, T. Z., and M. I. Richardson (1993), New dust opacity mapping from Viking Infrared Thermal Mapper data, *J. Geophys. Res.*, *98*(E6), 10,941–10,949.

Peterfreund, A. R., and H. H. Kieffer (1979), Thermal infrared properties of the Martian atmosphere: 3. Local dust clouds, *J. Geophys. Res.*, *84*(B6), 2853–2863.

Ryan, J. A., and R. M. Henry (1979), Mars atmospheric phenomena during major dust storms, as measured at surface, *J. Geophys. Res.*, *84*(B6), 2821–2829.

Schneider, E. K. (1983), Martian great dust storms: Interpretive axially-symmetric models, *Icarus*, *55*(2), 302–331.

Siili, T., R. M. Haberle, and J. R. Murphy (1997), Sensitivity of Martian southern polar cap edge winds and surface stresses to dust optical thickness and to the large-scale sublimation flow, in *Planetary Atmospheres and Ionospheres and Reference Atmospheres*, *Adv. Space Res.*, *19*, 1241–1244.

Smith, M. D., J. C. Pearl, B. J. Conrath, and P. R. Christensen (2000), Mars Global Surveyor Thermal Emission Spectrometer (TES) observations of dust opacity during aerobraking and science phasing, *J. Geophys. Res.*, *105*(E4), 9539–9552.

Smith, M. D., R. J. Conrath, J. C. Pearl, and P. R. Christensen (2002), Thermal Emission Spectrometer observations of Martian planet-encircling dust storm 2001A, *Icarus*, *157*(1), 259–263.

Thorpe, T. E. (1979), History of Mars atmospheric opacity in the southern hemisphere during the Viking extended mission, *J. Geophys. Res.*, *84*(A11), 6663–6683.

Tillman, J. E. (1988), Mars global atmospheric oscillations: Annually synchronized, transient normal-mode oscillations and the triggering of global dust storms, *J. Geophys. Res.*, *93*(D8), 9433–9451.

Toigo, A. D., M. I. Richardson, R. J. Wilson, H. Wang, and A. P. Ingersoll (2002), A first look at dust lifting and dust storms near the south pole of Mars with a mesoscale model, *J. Geophys. Res.*, *107*(E7), 5050, doi:10.1029/2001JE001592.

Wang, H., and A. P. Ingersoll (2002), Martian clouds observed by Mars Global Surveyor Mars Orbiter Camera, *J. Geophys. Res.*, *107*(E10), 5078, doi:10.1029/2001JE001815.

Wang, H., and A. P. Ingersoll (2003), Cloud-tracked winds for the first Mars Global Surveyor mapping year, *J. Geophys. Res.*, *108*(E9), 5110, doi:10.1029/2003JE002107.

Wang, H., M. I. Richardson, R. J. Wilson, A. P. Ingersoll, A. D. Toigo, and R. W. Zurek (2003), Cyclones, tides, and the origin of a cross-equatorial dust storm on Mars, *Geophys. Res. Lett.*, *30*(9), 1488, doi:10.1029/2002GL016828.

Wilson, R. J. (1997), A general circulation model simulation of the Martian polar warming, *Geophys. Res. Lett.*, *24*(2), 123–126.

Wilson, R. J., and K. Hamilton (1996), Comprehensive model simulation of thermal tides in the Martian atmosphere, *J. Atmos. Sci.*, *53*(9), 1290–1326.

Wilson, R. J., and M. I. Richardson (2000), The Martian atmosphere during the Viking mission, I - Infrared measurements of atmospheric temperatures revisited, *Icarus*, *145*(2), 555–579.

Zurek, R. W., and C. B. Leovy (1981), Thermal tides in the dusty Martian atmosphere: A verification of theory, *Science*, *213*(4506), 437–439.

————————————

S. P. Ewald, M. I. Richardson, and H. Wang, Division of Geological and Planetary Sciences, California Institute of Technology, MC 150-21, Pasadena, CA 91125, USA.

M. J. Strausberg, Department of Atmospheric and Oceanic Sciences, University of California, Los Angeles, 405 Hilgard Avenue, Box 951565, 7127 Math Sciences Building, Los Angeles, CA 90095-1565, USA. (mel@gps.caltech.edu)

A. D. Toigo, Graduate School of Science and Technology, Kobe University, Rokkodai-cho 1-1, Nada-ku, Kobe 657-8501, Japan.